M 2020

U.PORTO
FEUP FACULDADE DE ENGENHARIA
UNIVERSIDADE DO PORTO

CO PRODUCTION VIA REVERSE WATER-GAS SHIFT REACTION FOR FISCHER-TROPSCH APPLICATIONS

MARIA DA LUZ PAIS VENDAS

DISSERTAÇÃO DE MESTRADO APRESENTADA
À FACULDADE DE ENGENHARIA DA UNIVERSIDADE DO PORTO EM
CHEMICAL ENGINEERING

Master's in chemical engineering

CO production via Reverse Water-Gas Shift Reaction for Fischer-Tropsch Applications

Master dissertation

of

Maria Vendas

Developed within the course of dissertation

held in

DMT Environmental Technology / R&D Department

Supervisor at FEUP: **Prof. Alexandre Ferreira**

Supervisor at DMT Environmental Technology: **MSc. Benny Bakker**

U.PORTO
FEUP FACULDADE DE ENGENHARIA
UNIVERSIDADE DO PORTO

DEPARTAMENTO DE
ENGENHARIA QUÍMICA

April 2021

‘Whatever you do in life, keep on laughing’
-Gerrit Wigger

Acknowledgment

In this section, I would like to thank all the people that, one way or another, were involved and contributed to the accomplishment of this work.

To my supervisor Dr. Alexandre Ferreira, I would like to express my kind acknowledgments for all the availability and willingness to help, orientate and instruct me. Even though the distance was an inevitable problem, his effort and availability made me feel at home.

A special thanks to my supervisor Benny Bakker for all the support, to kindly share his knowledge and experience with me, and for closely monitor my work at DMT Environmental Technology. Also, to Maria Marcela Fragozo, I would like to give a particular thanks for all the technical support and concern in helping me to improve my work and to start thinking like an engineer.

To turn this internship into a life experience, thanks to the people that shared this last six months with me. Ana Cancela, Débora Luiz and Sofia Sousa, thanks for making my days enjoyable. It was a pleasure to share this experience with you.

I would like to give a special thanks to André Sousa for always be by my side.

Finally, endless thanks to my parents that always believed in me and supported me. I owe both too much to express in words.

Abstract

Climate changes, due to anthropogenic activities, are one of the main concerns nowadays. From the industrial processes, passing through excessive combustion of fossil fuels, to the greenhouse gases released and its contribution to CO_2 concentration in the atmosphere, are the main reasons that led to the environmental problem that mankind is facing.

The increasing mobility of populations is one of the most impacting activities and an essential characteristic of modern society, leading to increased fossil fuel energy demand.

Therefore, biokerosene as a sustainable fuel has stated an essential position concerning the carbon footprint associated with common fossil fuels, especially in the last few years.

Due to low-efficiency rates and the need of high capital investments of competing technologies, the reverse water-gas shift (rWGS) and the Fischer-Tropsch process emerge as the prominent technology for converting CO_2 into CO and CO into liquid fuels (diesel, gasoline, kerosene, etc.).

This work aims to present a sustainable alternative biokerosene production through the reverse water-gas shift (rWGS) reaction and the Fischer-Tropsch (FT) synthesis. The focus of this thesis lies on the production of CO with renewable H_2, from electrolysis process, and biogenic CO_2, obtained via direct air capture (DAC) or as a by-product from biogas upgrading, to further integrate the FT process to accomplish the sustainable production of 50 litters of biokerosene per day, at the pilot-scale.

To achieve this work objectives, first, it was defined the kinetic model to describe the reactive system, with the respective validation. The simulation was conducted resorting to the software Aspen Plus V12, and the results show a CO production of 1.93×10^{-3} kmol·h^{-1}, accomplished in a reactor with 0.25 meters length and 0.026 meters for the diameter. It was also studied the effect of the integration of an inert stream (N_2) in the process, to reduce the residence time.

Additionally, a water removal unit was added to separate the produced water from the remaining compounds with a separation percentage near 99%.

Keywords: **rWGS, CO production, syngas, biokerosene, Fischer-Tropsch**

Resumo

Alterações climáticas, derivadas das atividades do ser humano, são uma das principais preocupações nos dias que correm. Desde os processos industriais, passando pela combustão excessiva de combustíveis fósseis, à libertação de gases de efeito de estufa e a sua contribuição para o problema concentração de CO_2 na atmosfera, são umas das principais razões que levaram ao problema ambiental que o ser humano está a enfrentar.

O aumento da mobilidade das populações é uma das atividades mais impactantes e uma caraterística importante da sociedade moderna, levando a um aumento da procura da energia proveniente de combustíveis fósseis.

Sendo assim, o bio queroseno como um combustível sustentável ganhou uma posição relevante, no que diz respeito à pegada de carbono associada aos combustíveis fósseis mais comuns, especialmente nos últimos anos.

Devido a uma baixa eficiência e à necessidade de um investimento de capital elevado para alcançar uma competitividade tecnológica, os processos rWGS e FT emergem como tecnologias proeminentes na conversão de CO_2 em CO e, posteriormente, o CO em combustíveis líquidos (diesel, gasolina, queroseno, etc).

Este trabalho ambiciona apresentar uma alternativa sustentável para a produção do bio queroseno através da reação rWGS e da síntese FT. O foco desta tese assenta na produção de CO a partir de H_2 renovável, proveniente do processo de eletrólise, e de CO_2 biogénico, obtido a partir captura direta de ar (CDA) ou como um subproduto proveniente do pós-tratamento do biogás, para posteriormente integrar o processo FT com o intuito de alcançar uma produção sustentável, à escala piloto, de 50 litros de bio queroseno por dia.

De forma a atingir o objetivo deste trabalho, primeiramente foi definido um modelo cinético para descrever o sistema reativo, com respetiva validação. A simulação foi conduzida recorrendo ao programa Aspen Plus V12 e os resultados demonstram uma produção de CO de $1{,}93 \times 10^{-3}\,kmol \cdot h^{-1}$, num reator de 0,25 metros de comprimento e 0,026 metros de diâmetro. Foi também estudado o efeito da integração de uma corrente de inerte (N_2) no processo, com o objetivo de reduzir o tempo de residência.

Adicionalmente, foi adicionada uma unidade de remoção de água para separação dos restantes componentes, com uma percentagem de separação próxima de 99%.

Palavras-Chave: **rWGS, produção de CO, gás de síntese, bio queroseno, Fischer-Tropsch**

Declaration

I hereby declare, under word of honour, that this work is original and that all non-original contributions is indicated and due reference is given to the author and source

Sign and date

17 of march of 2021

Index

List of Figures

List of Tables

Notation and Glossary

D	Diameter	m
E_j	Activation energy of the reaction j	$kJ \cdot mol^{-1}$
F_i	Molar feed rate of the component i	$kmol \cdot h^{-1}$
f_i	Molar flow of the component i	$kmol \cdot h^{-1}$
H_j	Enthalpy of the reaction j	$kJ \cdot mol^{-1}$
K_j	Equilibrium constant of the reaction j	$-_{,where\ j=1}$ $bar^{2}_{,where\ j=2,3}$
K_i	Adsorption constant of the component i	$-_{,where\ i=H_2O}$ $bar^{-1}_{,where\ i=CH_4,CO,H_2}$
k_j	Rate coefficient of the reaction j	$kmol \cdot bar^{-1} \cdot kg_{cat}^{-1} \cdot h^{-1}_{,where\ j=1}$ $kmol \cdot bar^{1/2} \cdot kg_{cat}^{-1} \cdot h^{-1}_{,where\ j=2,3}$
l	Length	m
P	Pressure	bar
p_i	Partial pressure of the component i	bar
T	Temperature	K
T_{ref}	Reference temperature	K
R	Ideal gas constant	$m^3 \cdot Pa \cdot K^{-1} \cdot mol^{-1}$
r_j	Reaction rates of the reaction j	$kmol \cdot kg_{cat}^{-1} \cdot h^{-1}$
V	Volume	m^3
W	Weight of catalyst	kg
x_i	Molar fraction of the component i	-

Greek Letters

α	chain growth probability	-
Δ	concentration of the active sites	-
ε_b	bed porosity	-
ρ	density	$kg \cdot m^{-3}$
ξ	extent of the reaction	$kmol \cdot h^{-1}$
τ	residence time	s^{-1}
υ	stoichiometric number	-
χ	conversion	%

Indexes

i	Components
j	Reaction number
n	Number of carbons

List of Acronyms

ASF	Anderson-Schulz-Flory
AtJ	Alcohol to Jet
ASTM	American Society for Testing and Materials
CCS	Carbon Capture and Storage

DAC	Direct Air Capture
DSHC	Direct Sugar to Hydrocarbons
FT	Fischer-Tropsch
GHG	Greenhouse Gas
HEFA	Hydrogenated Ester and Fatty Acids
HTFT	High-Temperature Fischer-Tropsch
HoQ	House of Quality
LHHW	Langmuir-Hinselwood-Hougen-Watson
LTFT	Low-Temperature Fischer-Tropsch
PFD	Process Flow Diagram
RDT	Rate-Determining Step
RWGS	Reverse Water-Gas Shift
SIP	Synthetized Iso-Paraffins
SKA	Synthetic Paraffinic Kerosene with Aromatics
SPK	Synthetic Paraffinic Kerosene
SRM	Steam Methane Reforming
WGS	Water-Gas Shift

1 Introduction

1.1 Framing and presentation of the work

During the last years, human activities have been the main contribution to releasing greenhouse gases into the atmosphere, and it tends to increase, as evolution takes place. Non-sustainable consumption of fossil-fuels linked with environmental threats from its exploration is an emergent concern and efforts must be combined to achieve a solution able to provide clean and renewable energy sources.

The transportation sector turns out to be one of the main contributors to global warming. So, it is imperative to focus on providing alternative energy sources to reduce greenhouse gas (GHG) emissions. [1] Financially, as crude oil is a scarce resource, the emergence of an alternative solution is also essential to face the rising costs of crude oil in the future.

Carbon dioxide global emissions contribute to the biggest piece of global GHG emissions into the atmosphere. It represents more than 60% of the greenhouse worldwide effect, and, considering only industrialized countries, CO_2 represents over 80% of greenhouse gas emissions. [2]

Aviation activity is responsible for around 2% of the global CO_2 anthropogenic emissions, and 10% of the fuel consumption is achieved by the aviation sector. Even though the numbers already represent a concern, it is expected that the aviation sector doubles its activity within seven years from now, representing a consequent increase of the CO_2 emissions up to double in 25 years. [3]

Due to the negative environmental impact of this industry, the aviation sector has committed itself to reduce net emissions by 50% until 2050, compared to the emission levels of 2005. [4]

Although new technologies have a critical role in reducing CO_2 emissions, a large quantity of gases are still being produced and released into the atmosphere. To contribute to its decreasing, various carbon capture and storage (CCS) technologies are being developed during the past years. [5] The idea is to capture CO_2 from large industrial sources and then recycle it by converting it into high-value useful chemical products. [6]

This way, the conversion of CO_2 into CO, through the reverse water-gas shift (rWGS) reaction, has been taking as a promising process to produce syngas that, on the other hand, has a high value due to its importance on the Fischer-Tropsch (FT) process, to produce biofuels. [7]

The compounds generated in the synthesis consist mainly in linear-hydrocarbon chains with different lengths, fluctuating between 2 and 20 carbons, which includes fuels such as gasoline,

kerosene and diesel, and obey a relation called Anderson-Schulz-Flory (ASF) distribution, later explained in this work. The production of light gases is also present.

Franz Fischer and Hans Tropsch developed this synthesis, around 1920 in Germany, intending to produce liquid fuels from coal. Since then, this has been extensively studied and improved to achieve the most efficient process to transform CO_2 and H_2 into syngas and, finally, into biofuels.

Currently, this topic has become one of the most relevant for CO_2 recovery and utilization. Furthermore, the production of CO has an important role nowadays since CO is essential for the production of many chemical products and has endless applications in the industry. [8]

1.2 Presentation of the company

DMT Environmental Technology is a company specialized in developing innovative solutions for the environment, founded in 1987 by Rob Dirkse with the push of emergency of environmental clean-up technologies. A leader in the biogas upgrading market, the company also has a strong market not only in the technologies for water treatment (TurboTec) and gas desulfurization (Sulfurex) but also in membrane systems for biogas upgrading (Carborex).

Due to the current problem with greenhouse gas emissions, the company aims to state a position in the capture and utilization of CO_2 through biokerosene production to provide an environmentally friendly solution in the transportation sector and, this way, reduce the impact of aircraft engines in the worldwide emissions.

The company has a worldwide presence that is accomplished by over 100 employees and partners, offering efficient systems for all over the world and contributing positively to a sustainable and better future.

1.3 Contribution of the author to the work

The aim of this work is the production of biokerosene from renewable sources through rWGS and FT synthesis.

The present work represents the first step to achieve the production of biofuels with CO_2, captured from the atmosphere or from biogenic sources, such as biogas upgrading plants, and H_2, from renewable sources, which is believed to be the key to develop a sustainable carbon cycle with hydrogen generated from non-fossil energy, such as electrolysis.

The author's contribution is focused on the valorisation of CO_2 through the development of a rWGS reactor to produce CO. All the assumptions of the model, considerations and mathematical equations are presented and minutely explained.

1.4 Organization of the thesis

This dissertation is organized according to the following chapters:

In Chapter 1 it is given the contextualization of the work that will be carried throughout the dissertation.

In Chapter 2 is contemplated a summary of the rWGS and FT processes, conditions, and limitations, as well as the technologies and their evolution. Specific concepts and methods essential to carry the work are also explained in detail. An overview of the influence of parameters such as temperature, pressure, and residence time in the process is presented.

In Chapter 3 there is explained the methodology used to simulate the process on Aspen Plus V12 and the mathematical calculations to determine the parameters, as well as the assumptions that were taken. The selection of the kinetic model and its validation are presented throughout this chapter.

In Chapter 4 are presented the obtained results of the simulation for the studied case, as well as the influence of the evaluated parameters reviewed.

In Chapter 5 there are the conclusions obtained from this study, in addition to the future work that must be carried on this topic and recommendations.

In Chapter 6 is carried a final appreciation of the project and future prospects.

2 Context and State of the Art

Kerosene is a hydrocarbon chain composed between 10 and 16 carbons, typically characterized by molecules with an average carbon number of 12, that can be obtained from oil crude. The properties of kerosene are presented in Table 1. [9]

Table 1. Physical properties of kerosene at 25 °C and constant pressure.

Molecular Weight ($g \cdot mol^{-1}$)	Density ($g \cdot cm^{-3}$)	Melting Point (°C)	Boiling Point (°C)	Flash Point (°C)	Auto Ignition Temperature (°C)
170	0,808	-47	176	38	210

Specific Energy ($MJ \cdot kg^{-1}$)	Energy Density ($MJ \cdot L^{-1}$)	Lower Explosive Limit (vol%)	Upper Explosive Limit (vol%)	Vapor Pressure at 20°C (hPa)
37,43	34,9	0,6	6,5	3

2.1 Biokerosene Production Routes

The production of biokerosene can be achieved by different pathways. Therefore, different conversion routes are considered toward the production of biokerosene from different materials. The main transformation routes for the production of biokerosene are briefly explained in Annex A.

The final product depends on the conversion route and can be classified as synthetic paraffinic kerosene (SPK), synthetic paraffinic kerosene with aromatics (SKA), and synthesized iso-paraffins (SIP). The aromatic content on SPK and SIP fuels, according to the ASTM (American Society for Testing Materials) D7566 legislation, is limited to 0.5 vol.%. Even though the presence of aromatic content is significantly residual, its absence may lead to lubricity problems. [10, 11]

The produced biokerosene should be as close as possible to the commercial fuels applied in the aviation industry. Jet A-1 is the reference for this project, as this is one of the most used fuels in the aviation sector and has worldwide application. It is approximately the same as Jet A in terms of properties and characteristics. Still, Jet A-1 requirements include one or more additives not needed for Jet A. These additives allow a lower freezing point of the fuel, making it more proper for long flights, especially on cold routes in the winter. [12, 13]

The main properties of Jet A-1 are described in Table 2. [14]

Table 2. Jet A-1 properties.

Property	Jet A-1	Limit
Flash Point / ºC	48	> 38
Density at 15ºC / kg·m^{-3}	816	775 - 840
Freezing Point / ºC	-54.5	< -47
Viscosity at -20ºC / mm^2·s	4.08	< 8.0
Aromatics Content / vol.%	18.6	< 25
Sulphur Content / vol.%	0.00746	< 0.3

The composition of the Jet A-1 is described in Figure 1. [14]

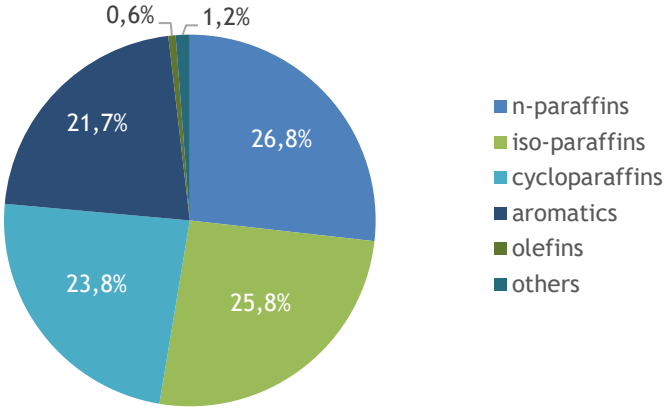

Figure 1. Jet A-1 reference composition.

On the one hand, the n-paraffins, iso-paraffins, and cycloparaffins are the most desired fraction to set the fuel due to the high amount of heat release per weight unit and burns cleanly. On the other hand, olefins presence gives place to good combustion, but its fraction is limited due to the risk of gum formation. Also, the presence of aromatics is not desirable, regard to combustion characteristics. The aromatic content leads to poor combustion, burns with a smoky flame and releases more chemical energy, comparing with the other hydrocarbons. [13]

2.2 Fischer-Tropsch

FT synthesis is the most studied route for biokerosene production and is defined as simultaneous or successive chemical reactions responsible for the conversion of CO and H_2 into liquid hydrocarbon products divided mainly into naphtha (C_4-C_9), kerosene (C_9-C_{16}), and diesel (C_9-C_{20}). Described as the catalytic hydrogenation of CO, the Fischer-Tropsch has as its main objective the production of a wide range of products with high commercial value.

The reaction set that described this extremely exothermic process is presented in Eq. 2.1 and Eq. 2.2, respectively, the production of paraffins and olefins. [15]

$$(2n+1)\,H_2 + nCO \rightarrow C_nH_{2n+2} + nH_2O \quad 2.1$$

$$2nH_2 + nCO \rightarrow C_nH_{2n} + nH_2O \quad 2.2$$

In the FT process, there are side reactions, such as the formation of alcohols, described by Eq. 2.3. The production of CO_2 can also occur spontaneously due to the presence of CO and H_2O in the reactor through the WGS reaction, represented in Eq. 2.4.

$$nCO + 2nH_2 \rightarrow C_nH_{2n+1}OH + (n-1)H_2O \quad 2.3$$

$$CO + H_2O \rightarrow CO_2 + H_2 \quad 2.4$$

The Boudouard reaction, represented by Eq. 2.5, is also likely to occur and lead to the production of coke.

$$2CO \rightarrow C + CO_2 \quad 2.5$$

The coke formation is hazardous due to the possibilities of catalyst poisoning and blocking of the active sites.

The FT process is presented in Figure 2. [16]

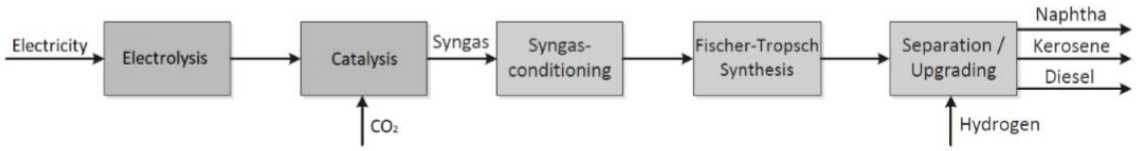

Figure 2. FT synthesis PFD.

2.2.1 Temperature

Depending on the process operating temperature, two types of FT synthesis can be distinguished: low and high temperature. The low-temperature Fischer-Tropsch (LTFT) generally occurs in a range of temperatures between 200 and 250 °C, favouring the production of liquid fuels up until middle distillates. [17] On the other hand, the high-temperature Fischer-Tropsch (HTFT), which is operated between 300 and 350 °C, favours the production of gas products, such as methane, and lower distillates.

Generally, the FT process for kerosene production is operated in LTFT, reducing this way energy costs, and at high pressures, between 20 and 40 bar. [18] The H_2/CO molar ratio feed into the reactor is around 2, to achieve a higher proportion of liquid fuels as possible. [19]

This synthesis process is controlled by the chain growth probability, α. This value quantifies approximately the range of products obtained at the end of the synthesis. [20] For the Fischer-

Tropsch, it is considered the Anderson-Schulz-Flory product distribution model, that traduces the mole fraction distribution of products as function of the number of carbon atoms in the chain. It is described according to Eq. 2.6. [21]

$$X_n = \alpha^{n-1}(1-\alpha) \qquad 2.6$$

The α value depends on various conditions, where the main are temperature, pressure, and catalyst. For the production of long-chain hydrocarbons, as biokerosene, the value of α should be close to 1 and, to achieve high α values, low-temperature processes are preferable, as possible to observe in Figure 3. [22–25]

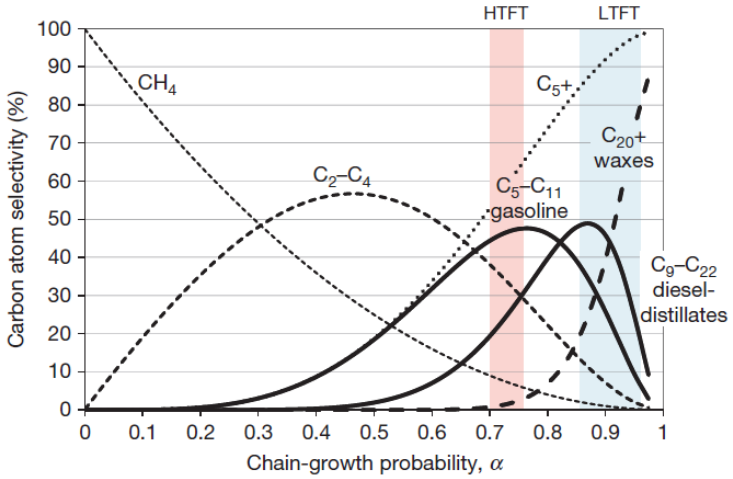

Figure 3. FT products according to the chain growth probability, α.

The catalyst applied are, typically, Co and Fe-based catalysts since Ru is very expensive. As Fe catalysts have an essential role in promoting the WGS reaction, which leads to the production of CO_2 and consequent consumption of CO, usually, Co-based catalysts are preferable for biofuel production.

In Appendix A is presented a house of quality (HoQ) for the selection of the best catalysts.

Thus, with a Co catalyst, temperatures between 200 and 250 °C and around 40 bar, the process is expected to achieve a α value close to 0,9. [10]

During the last years, several reactors were studied and developed different reactor technologies to perform the highly exothermic production of biokerosene. Even though the conventional models (fluidized-bed, slurry-phase, and multitubular fixed-bed) are the most applied in industry, alternative reactors have been the focus to improve the performance of the conventional ones and, that way, increase the hydrocarbon production and suppress the CH_4 and CO_2 formation during the FT process.

2.2.2 Membrane Reactor

Recently, the scientific community is trying to develop a membrane reactor to use only a single reactor instead of two (rWGS reactor and FT reactor) for the production of biokerosene.

The concept of these reactors is to shift the chemical equilibrium towards the desired product by selectively feeding or removing one or several components. Consequently, higher specific production rates, higher catalyst lifetimes and higher product selectivity are accomplished. Membrane reactors may have great potential, especially for small-medium scale FT units.

Considering the different properties of the membranes, different final results can be obtained in the FT synthesis. There are four different membranes reported in the literature, but the *in situ* water removal is the most studied and promising. [21, 26] The following Figure 4 represents the process and the operation steps of a membrane. [27]

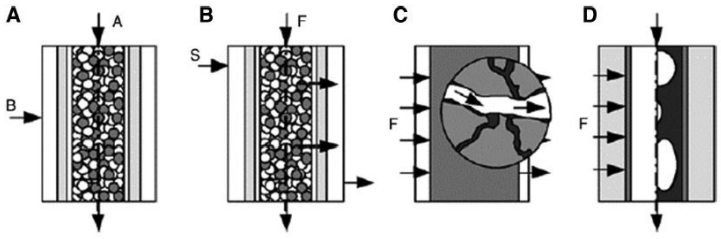

Figure 4. Membrane reactors for FT synthesis.

In Appendix B is presented a house of quality analysis for the selection of the best reactor.

2.3 Reverse Water Gas Shift Reaction

The rWGS reaction is required for the production of syngas in the concept of the renewable FT process. This is an essential step to produce CO to feed to the FT reactor and then produce biokerosene. The process flow diagram (PFD) is presented in Appendix C.

Even though the primary process to produce syngas is the steam methane reforming (SMR), as in this study the feed gases are renewable H_2 and CO_2 captured from the atmosphere, the process applied to this transformation is the rWGS.

The reactant CO_2 is known as a highly stable molecule, which means that it requires a significant amount of energy, high temperatures and the use of active catalysts for its efficient conversion into CO. [28]

The endothermic rWGS reaction is described in Eq. 2.7:

$$CO_2 + H_2 \rightleftarrows CO + H_2O \qquad \Delta H^0_{298} = 42.1\ \text{kJ} \cdot \text{mol}^{-1} \tag{2.7}$$

As this is an equilibrium reaction, the opposite reaction, water-gas shift (WGS) reaction, represented by Eq. 2.8, is likely to happen in the reactor.

$$CO + H_2O \rightleftarrows CO_2 + H_2 \qquad \Delta H_{298}^0 = -42.1\ \text{kJ} \cdot \text{mol}^{-1} \qquad 2.8$$

Besides this reaction, it is crucial to notice that there are side reactions that may also occur apart from the WGS. Therefore, the main reactions considered suitable to happen are the Sabatier (or CO_2 methanation), CO methanation, Bosh and Boudouard reactions, leading to the formation of undesirable products, such as CH_4 and coke. The reactions mentioned are respectively represented by Eq. 2.9, 2.10, 2.11, and 2.12.

$$CO_2 + 4H_2 \rightleftarrows CH_4 + 2H_2O \qquad \Delta H_{298}^0 = -165.0\ \text{kJ} \cdot \text{mol}^{-1} \qquad 2.9$$

$$CO + 3H_2 \rightleftarrows CH_4 + H_2O \qquad \Delta H_{298}^0 = -206.5\ \text{kJ} \cdot \text{mol}^{-1} \qquad 2.10$$

$$CO_2 + 2H_2 \rightleftarrows C + 2H_2O \qquad \Delta H_{298}^0 = -90.2\ \text{kJ} \cdot \text{mol}^{-1} \qquad 2.11$$

$$2CO \rightleftarrows C + CO_2 \qquad \Delta H_{298}^0 = -172.6\ \text{kJ} \cdot \text{mol}^{-1} \qquad 2.12$$

The formation of coke is hazardous for the catalyst due to its tendency to block the active sites and, consequently, result in the loss of the catalyst activity. [29, 30]

However, as the reactor operation conditions are established to favour the rWGS and the production of CO, as the side reactions are exothermic and so are suppressed by the increase of the temperature, it is crucial to understand the extension of all the possible reactions. The analysis of this potential problem is presented in Chapter 4.1.

2.3.1 Temperature

As the CO_2 molecule presents high stability, high temperatures are needed to move the thermodynamic equilibrium of the rWGS towards the production of CO. According to the previous studies, CH_4 and coke molecules are only stable, respectively, at temperatures below 700 and 900 °C, even though coke formation is not likely to occur, according to its kinetics. [31] Thus, high temperatures are needed to suppress the two by-products formation, unwanted and harmful to the catalyst, particularly coke formation, due to its probability of lead to catalyst coking during the process, especially when operating with low H_2/CO_2 ratios. [31, 32]

In Figure 5, there is represented the equilibrium obtained at different temperatures.

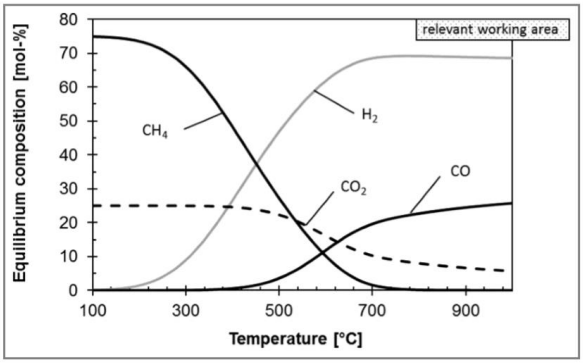

Figure 5. Influence of the temperature in the rWGS equilibrium.

However, the temperature should be kept as low as possible to decrease energy losses and minimize capital costs. Considering equilibrium compositions in Figure 5, it is demonstrated that above 700 °C, the fraction of CH_4 is neglectable, and the CO is close to the maximum value. Then, the temperature oscillating between 700 and 1000 °C should be the reference range to operate. This study will be conducted at 700 °C.

2.3.2 Pressure

According to the Le Chatelier principle, the equilibrium composition is characterized by the increase or decrease of the number of moles of a reaction. Taking into account this information and considering the present reactive system, the pressure will not affect the rWGS reaction, as the sum of the number of moles of the products and the reactants are the same. However, for the methanation reactions, the increase of the pressure will move the reaction towards the production of CH_4 and H_2O since the sum of the number of moles of the products is smaller. [33]

In Figure 6, it is possible to observe the influence of the pressure and temperature in the overall CO_2 conversion and confirm the tendency stated before. [33]

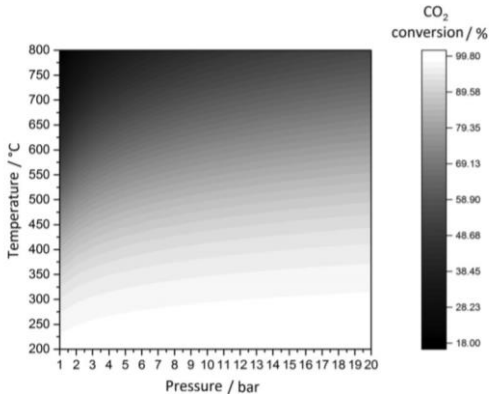

Figure 6. Effect of the pressure and temperature in the thermodynamic CO_2 conversion.

Even though the increase of the pressure favours the production of CH_4, experiments conducted by Xu and Froment show that the influence of the pressure between 1 and 30 bar can be neglected, as the differences in the final conversion and selectivity are not that significant. [34]

Furthermore, previous studies show that high pressures lead not only to elevated CO_2 conversions but also high CO selectivity and low CH_4 selectivity. This tendency is possible to observe in Figure 7. [35]

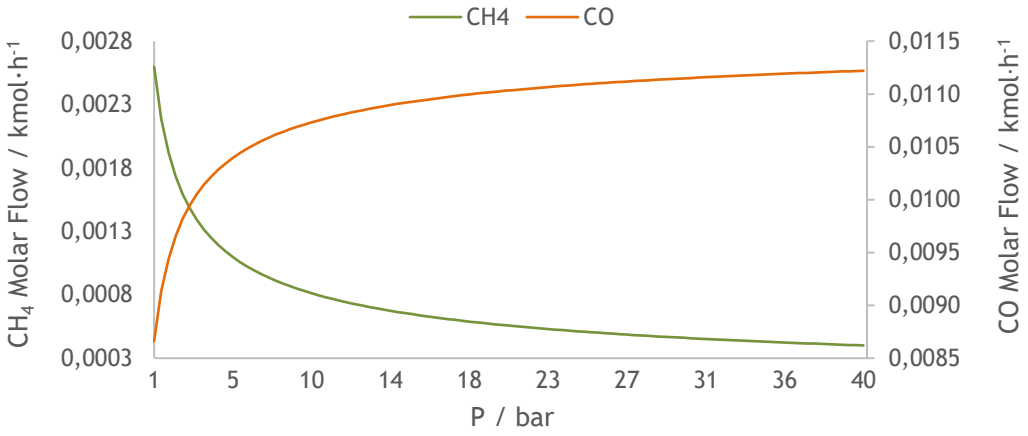

Figure 7. CO and CH_4 molar flow as a function of the pressure.

Considering that the production of CO through the rWGS is preceding the FT synthesis since the pressure does not significantly influence the chemical equilibrium, it is profitable to operate the rWGS reactor at the same pressure as the FT reactor. Therefore, as the FT reaction, using a Co-based catalyst, requires high pressures, it simplifies the operation to apply the same pressure at the rWGS step, having then the compression stage before the rWGS instead of between the two reactors, which would require additional cooling, compression and reheating processes. [34, 36] In this study, as the FT synthesis will be conducted under 24 bar, the rWGS will be operated at the same pressure.

2.3.3 Residence Time

As expected, when it is noticed an increase in the residence time, the overall CO_2 conversion immediately tends to increase as well, which is demonstrated in Figure 8. [33]

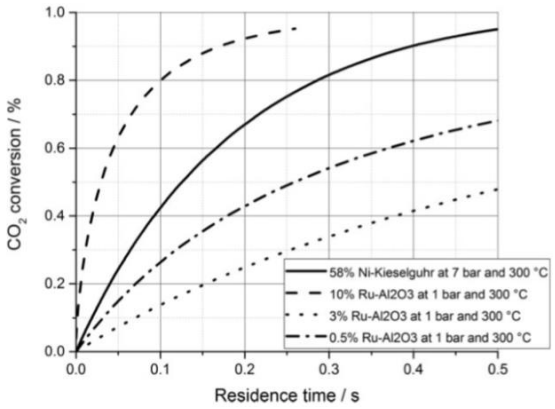

Figure 8. CO_2 conversion as a function of the residence time.

As the kinetics of the rWGS is fast, the residence time of the CO_2 and H_2 molecules should be short, between 5 and 64 ms, to achieve the maximum conversion of CO_2 towards the production of CO. [28]

On the other hand, if the residence time increases, the selectivity towards CH_4 will consequently increase. As the methanation reaction has slower kinetics, increasing the residence time above 64 ms provides enough time for the production of CH_4, which is not desirable.

With the aim to decrease the residence time inside the reactor, it is often added to the feed an inert, usually nitrogen, to assure that the reaction has an elevated intrinsic velocity, and consequently, short residence times. In the following Figure 9, the reduction of the CO_2 conversion, and CO selectivity with the rise of the residence time on the rWGS reaction is observed. [37]

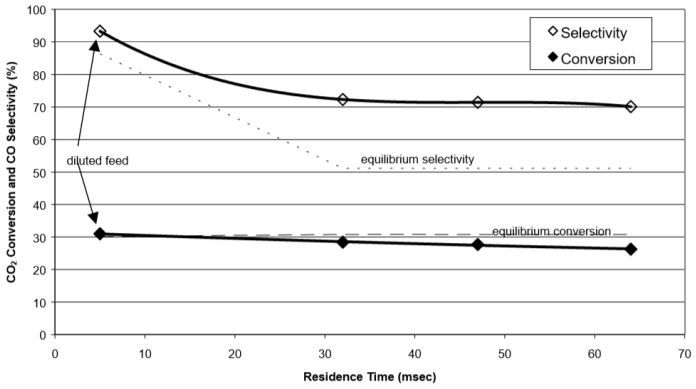

Figure 9. Equilibrium conversion and CO selectivity for rWGS reaction.

2.3.4 Inlet Ratio

According to the thermodynamic, the conversion of CO_2 into CO through the rWGS reaction is enhanced when the H_2 is feed in excess. [28] Usually, the H_2/CO_2 ratio applied in this process

is 3. Operating with an excess of hydrogen also helps to prevent carbon deposition on the catalyst surface.

2.3.5 Catalyst

It is essential to understand which catalyst is associated with the higher productivity to generate the maximum fraction of the desired product, which, in this study, is CO for the production of biokerosene. [15, 27]

Several metals have been studied during the past years to understand which is the best catalyst for the rWGS reaction. Several authors defined the activity of the metals according to Ru > Fe > Ni > Co > Rh > Pd > Pt > Ir. [33, 38]

Even though Ru is the metal that presents better characteristics, such as the resistance to oxidation, it is very expensive and so limits its application in industrial processes. Therefore, typical catalysts for this process are Ni-based due to their high activity linked with low cost and high availability. [39–41] Compared to Ni, Fe catalysts, besides presenting an excellent CO_2 conversion, are very cheap. However, at low-temperatures, enhance the CH_4 production, which is not desired for this synthesis.

The characteristics of a good catalyst for the rWGS reaction are not particularly different from those of catalytic materials for conventional high-temperature reactions. Hereupon, an active phase dispersion, local microstructure, high porosity, high thermal stability and mechanical stability are the main properties required for the syngas synthesis. [42] Also, the resistance to deactivation for carbon formation or sintering are essential characteristics. [43]

The most common catalysts selected to catalyse this reactive system, due to their attractive activity-price relationship, are the Ni/Al_2O_3 based catalysts. This catalyst is highly reactive, even though it promotes a minimal methane formation during the CO synthesis, even when the process is conducted at low-temperatures.

Due to high nickel dispersion and basicity, this catalyst showed a high rate of CO_2 conversion near the equilibrium conversion, around 40%, and an even higher CO selectivity, near 100%. [15, 16, 44] Also, Ni-based catalysts present low selectivity to methane, which is an advantage since the production of CH_4 is undesired for the process.

However, the Ni content must remain lower than 2%; otherwise, the methanation reactions are favoured, especially when operating at low-temperatures. This is shown in Figure 10. [35]

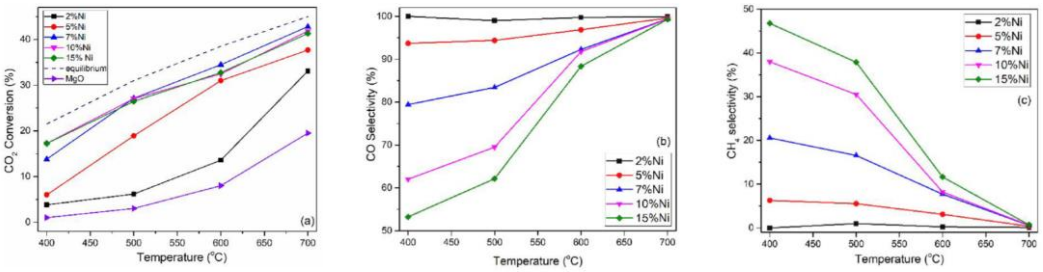

Figure 10. The variance of a) CO_2 conversion, b) CO selectivity and c) CH_4 selectivity according to the Ni content.

The main advantage of Ni as a catalyst is the presence of good hydrogenation behaviour and high stability at high temperatures, as the melting point is 1455 °C. [45]

Due to its high specific surface area, narrower pore size distribution and lower total pore volume, this catalyst leads to a high conversion of CO_2. [35]

Even though the slight tendency to produce CH_4, when operating at low-temperatures, Ni is the best candidate for the rWGS due to the high operating temperatures required. According to Gibbs equilibrium calculations, the methanation reaction is strongly favoured at low-temperatures, below 350 °C, completely different from the operating temperature range. [46]

2.3.6 Support

Nonetheless, the implementation of a support structure has a crucial role in backing the catalytic reaction, to achieve the range of desired products. In addition to support, the use of specific promoters may offer desirable features to the catalyst, such as increase the reaction rate, improve the stability and the selectivity of the desired compounds. Thermal stability and coke resistances are the main reasons to justify the use of different support materials. [47] Previous studies show that catalysts with support materials improve the ability to limit carbon formation. [48–51]

For the production of CO through the rWGS reaction, the role of alumina as support is essential. The dilution of the Ni catalyst in alumina prevents possible runaway situations, as the reaction requires high temperatures, operating in almost isothermal conditions thought the catalyst bed.

Moreover, the dilution of the catalyst in an inert material allows not only a uniform gas flow but also prevents high-pressure drops along the catalyst bed. That dilution contributes to a local decrease of the active sites' density. Consequently, the reaction is more homogeneous distributed along the catalyst bed and not only at the feeding region. [52, 53]

3 Materials and Methods

3.1 Kinetic Model

Although many studies for the rWGS have been done during the past decades, there are still disagreements and contradictory reports over the active sites and the reaction mechanism.

Several mechanisms, rate-determining steps and assumptions related to the active sites of the catalyst have led to many different rate expressions to describe the rWGS reaction. Considering all the probable conditions for each reaction and assumptions, the rate equation is generally arranged according to Yang and Hougen tables. As this is a complex reaction system, the rate equations cannot be constructed based on Yang and Hougen tables, and a different method is necessary for this situation.

One crucial aspect to approximate the simulation to the actual situation as much as possible is to select a kinetic model that is performed to predict the reaction mechanisms, and models found in the literature have already been validated with experimental data.

The kinetics of this reactive system has been extensively studied during the past years, leading to diverse mechanisms. [34, 54] Therefore, due to different assumptions and considerations on the reactions, various rate expressions can be derived, due to the many determining steps and assumptions defined. [55] The models presented in this document all consider not only the rWGS, but also the methanation reactions.

The simpler model to describe the reactions inside the rWGS reactor is the power-law model. [34] According to this model, the rWGS, CO_2 and CO methanation reaction rate equations are presented in Table 3.

Table 3. Rate equations for rWGS, CO_2 and CO methanation reactions based on the power-law model.

rWGS	CO_2 Methanation	CO Methanation
$r_1 = k_1(T)\left(P_{H_2}P_{CO_2} - \frac{P_{H_2O}P_{CO}}{K_1}\right)$	$r_2 = k_2(T)\left(P_{H_2}{}^4P_{CO_2} - \frac{P_{H_2O}{}^4P_{CH_4}}{K_2}\right)$	$r_3 = k_3(T)\left(P_{H_2}{}^3P_{CO} - \frac{P_{H_2O}P_{CH_4}}{K_3}\right)$

Based on the Langmuir-Hinselwood-Hougen-Watson (LHHW) model, there have been mechanisms, and rate equations developed to describe the reactive system analyzed in this study. [54] Xu and Froment developed a model based on the LHHW model. The rate equations are presented in Table 4.

Table 4. Rate equations for RWGS, CO_2 methanation and CO methanation reactions based on Xu and Froment's model.

rWGS	CO_2 Methanation	CO Methanation
$r_1 = \frac{\frac{k_1}{P_{H_2}}\left(\frac{P_{CO}P_{H_2}}{K_1} - P_{CO}P_{H_2O}\right)}{DEN^2}$	$r_2 = \frac{\frac{k_3}{P_{H_2}^{3.5}}\left(\frac{P_{CO}P_{H_2}^{4}}{K_2} - P_{CH_4}P_{H_2O}^{2}\right)}{DEN^2}$	$r_3 = \frac{\frac{k_3}{P_{H_2}^{2.5}}\left(\frac{P_{CO}P_{H_2}^{3}}{K_3} - P_{CH_4}P_{H_2O}\right)}{DEN^2}$

$$DEN = \left[1 + K_{CO}P_{CO} + K_{H_2}P_{H_2} + K_{CH_4}P_{CH_4} + \frac{K_{H_2O}P_{H_2O}}{P_{H_2}}\right]$$

3.1.1 Selection and Description

From all the kinetic models presented in the literature, Xu and Froment model was demonstrated to be the most general and it is concluded to be the most suitable to describe the rWGS process at high temperatures, over a nickel catalyst. [56] Also, this model has been extensively investigated and successfully tested under laboratory conditions. [57]

According to the literature, this is considered the best kinetic model to represent the three-reaction system, represented below, in Figure 11. [34, 58]

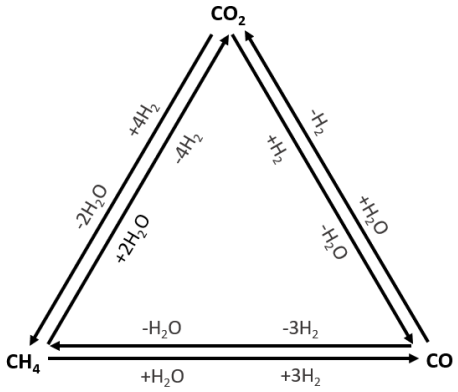

Figure 11. Reaction system scheme.

For the development of this model, Xu and Froment considered the following assumptions:

1. All the reactions occur on similar nickel-metal active sites
2. Water is adsorbed dissociative, yielding to adsorbed oxygen and hydrogen
3. Hydrogen is adsorbed dissociatively
4. Methane is adsorbed molecularly
5. The following carbon intermediates are formed:
   CH_4*, CH_3*, CH_2*, $CH*$ and $C*$, whose concentrations are much lower than the total concentration of the active sites
6. The following carbon and oxygen intermediates are formed:

CH_2O*, $CHO*$, $CO*$ and CO_2*

7. All the reaction schemes are thought to have a step for the main reactions with a considerably slower rate when compared to the other steps, and it is called the rate-determining step (RDT)

Considering the aforementioned conditions, the kinetic mechanisms for this reaction are described as:

Step	Reaction	I	II	III	
1.	$H_2 + * \rightleftarrows H_2*$	0	2	2	
2.	$H_2* + * \rightleftarrows 2H*$	0	2	2	
3.	$CO_2 + * \rightleftarrows CO_2*$	1	1	0	
4.	$CO + * \rightleftarrows CO*$	-1	0	1	
5.	$CO_2* + H* \rightleftarrows CHO* + O*$	0	1	0	RDS of r_2
6.	$CO_2* + * \rightleftarrows CO* + O*$	1	0	0	RDS of r_1
7.	$CO* + H* \rightleftarrows CHO* + *$	0	0	1	RDS of r_3
8.	$CHO* + H* \rightleftarrows CH_2O* + *$	0	1	1	
9.	$CH_2O* + * \rightleftarrows CH_2* + O*$	0	1	1	
10.	$CH_2* + H* \rightleftarrows CH_3* + *$	0	1	1	
11.	$CH_3* + H* \rightleftarrows CH_4* + *$	0	1	1	
12.	$CH_4* \rightleftarrows CH_4 + *$	0	1	1	
13.	$O* + H_2 \rightleftarrows H_2O + *$	1	2	1	

According to the reaction scheme represented and the mechanism described, the rate equations can be derived and written based on the rate-determining step of each rWGS reaction, CO_2 and CO methanation, respectively the reaction 6, 5, and 7, represented above, in terms of partial pressures and adsorbed species. [56]

Owing to the LHHW equilibrium relations, the following equations were derived, considering not only the partial pressures of the reactants, but also the balance of the active sites, including the vacate and those covered with adsorbed species. The final rate equations are represented,

for the rWGS, CO_2 and CO methanation reactions, respectively by Eq. 3.1, 3.2 and 3.3. All the intermediate steps performed to obtain the final rate equations are explicit in Appendix D.

$$r_1 = \frac{\frac{k_1(T)}{P_{H_2}}\left(\frac{P_{H_2}P_{CO_2}}{K_1} - P_{H_2O}P_{CO}\right)}{\left(1 + K'_{CO}P_{CO} + K_{H_2}P_{H_2} + K_{CH_4}P_{CH_4} + \frac{K'_{H_2O}P_{H_2O}}{P_{H_2}}\right)^2} \quad 3.1$$

$$r_2 = \frac{\frac{k_2(T)}{{P_{H_2}}^{3.5}}\left(\frac{{P_{H_2}}^4 P_{CO_2}}{K_2} - {P_{H_2O}}^2 P_{CH_4}\right)}{\left(1 + K'_{CO}P_{CO} + K_{H_2}P_{H_2} + K_{CH_4}P_{CH_4} + \frac{K'_{H_2O}P_{H_2O}}{P_{H_2}}\right)^2} \quad 3.2$$

$$r_3 = \frac{\frac{k_3(T)}{{P_{H_2}}^{2.5}}\left(\frac{{P_{H_2}}^3 P_{CO}}{K_3} - P_{H_2O}P_{CH_4}\right)}{\left(1 + K'_{CO}P_{CO} + K_{H_2}P_{H_2} + K_{CH_4}P_{CH_4} + \frac{K'_{H_2O}P_{H_2O}}{P_{H_2}}\right)^2} \quad 3.3$$

This way, it is possible now to describe the CO_2 consumption, as well as the CO and CH_4 formation, respectively as follow:

$$r_{CO_2} = r_1 + r_2 \quad 3.4$$

$$r_{CH_4} = r_2 + r_3 \quad 3.5$$

$$r_{CO} = r_1 - r_3 \quad 3.6$$

To determine the kinetic and the adsorption constants, the temperature dependence correlations developed by Arrhenius and van't Hoof, respectively described, were used as represented in Eq. 3.7 and Eq. 3.8, respectively. [34, 58]

$$k'_j(T) = k'_{j,T_{ref}} \exp\left\{-\frac{E_j}{R}\left(\frac{1}{T} - \frac{1}{T_{ref}}\right)\right\} \quad 3.7$$

$$K_j(T) = K_{j,T_{ref}} \exp\left\{-\frac{\Delta H_j}{R}\left(\frac{1}{T} - \frac{1}{T_{ref}}\right)\right\} \quad 3.8$$

As the reactions involved in this system are equilibrium reactions, which means that occur in both direct and reverse way, if the system suffers a deviation in the inlet composition, the response will be in order to restore the equilibrium. Furthermore, it is important to understand that the compositions and concentration of the reactants and products influence the reaction kinetic and, consequently, the equilibrium constant. [59]

The remaining parameters needed to proceed with the study are clarified and recapped in Table 5. [34]

Table 5. Parameters for each reaction.

rWGS	CO_2 Methanation	CO Methanation
$k_{1,648} = 7.333$	$k_{2,648} = 2.54 \times 10^{-5}$	$k_{3,648} = 1.63 \times 10^{-4}$
$E_1 = 106\,206.92\ \mathrm{J/mol}$	$E_2 = 66\,830.77\ \mathrm{J/mol}$	$E_3 = 24\,361.54\ \mathrm{J/mol}$
$\Delta H_1 = 39\,076.92\ \mathrm{J/mol}$	$\Delta H_2 = -177\,069.23\ \mathrm{J/mol}$	$\Delta H_3 = -215\,738.46\ \mathrm{J/mol}$
$K_1 = 0.06594$	$K_2 = 6089.25\ \mathrm{bar}^2$	$K_3 = 76\,694.85\ \mathrm{bar}^2$

K_1, K_2 and K_3 are calculated for the reference temperature of 648 K, according to Eq. 3.9. [59]

$$K_j = \exp\left(\frac{\lambda_1}{T^2} + \frac{\lambda_2}{T} + \lambda_3\right) \quad 3.9$$

3.2 Model Validation

The validation of the selected model, developed by Xu and Froment, is divided into two steps: the dimensional analysis and the simulation in the program Aspen Plus V12, to guarantee and assure that the results obtained by the authors can be replicated with the information available and given in the literature.

3.2.1 Dimensional Analysis

To understand if the given equations r_1, r_2 and r_3 can be used or if it is needed rearrangement, it is essential to go through the dimensional analysis. The units of the parameters involved are defined in the Notation and Glossary Chapter.

Considering the units of the parameters in the rate equations, it is possible to proceed to the dimensional analysis. All the rate equations must have the units described in $kmol \cdot kg_{cat}^{-1} \cdot h^{-1}$.

As the denominator is common to all the expressions, it was analyzed first and separately.

$$DEN = 1 + bar \times \frac{1}{bar} + bar \times \frac{1}{bar} + bar \times \frac{1}{bar} + \frac{bar}{bar} = dimenssionless \quad 3.10$$

As shown in Eq. 3.10, all the parameters cancel each other, which means that the denominator is dimensionless. This first conclusion simplifies the analysis of the rate equations, and now it is only necessary to study the numerator of the rate equations, as it is now known that the denominator does not influence the units of the rate velocity.

For the rWGS reaction, the expression is:

$$r_1 = \frac{kmol}{kg_{cat} \cdot h \cdot bar} \frac{1}{bar} \times (bar \cdot bar - bar \cdot bar) = \frac{kmol}{kg_{cat} \cdot h} \quad 3.11$$

For the Sabatier reaction or CO_2 methanation, the expression is:

$$r_2 = \frac{\text{kmol} \cdot \text{bar}^{1/2}}{\text{kg}_{\text{cat}} \cdot \text{h}} \frac{1}{\text{bar}^{3.5}} \times \left(\frac{\text{bar}^4 \cdot \text{bar}}{\text{bar}^2} - \text{bar}^2 \cdot \text{bar} \right) = \frac{\text{kmol}}{\text{kg}_{\text{cat}} \cdot \text{h}} \quad 3.12$$

Finally, for the CO methanation, the expression is:

$$r_3 = \frac{\text{kmol} \cdot \text{bar}^{1/2}}{\text{kg}_{\text{cat}} \cdot \text{h}} \frac{1}{\text{bar}^{2.5}} \times \left(\frac{\text{bar}^3 \cdot \text{bar}}{\text{bar}^2} - \text{bar} \cdot \text{bar} \right) = \frac{\text{kmol}}{\text{kg}_{\text{cat}} \cdot \text{h}} \quad 3.13$$

As the units for the velocity rate equations are verified to be according to the expected, it is possible to use the expressions without further handling.

3.2.2 Replication of the Results and Comparison

Besides the dimensional analysis, it was considered essential to perform the verification of the information given in the literature and the validation of the results obtained by the replication of the simulation, to obtain approximately the same final conversions and mainly, to verify the same tendency: the increase of the production of CO with the rise in the temperature.

To confirm if the presented results of this study are supported by the data in the literature, a simulation was conducted respecting the parameters and conditions referred to in the literature, where the main objective is to obtain results close to the ones presented in the literature. This way, it is possible to rely on the information given and, finally, apply it in the reactor simulations, to attain the target product, CO, and integrating the Fischer-Tropsch process for the production of 50 $L \cdot day^{-1}$ of kerosene.

As referred, the software used in the present study to simulate the rWGS process is Aspen Plus V12, which allows the establishment of a theoretical environment operating in defined conditions, and provides close predictions of the results obtained in a real process.

The conditions defined by the authors for the reactor where the experimental ones from the literature, and are summarized in Table 6.

Table 6. Operation conditions and reactor dimensions.

P / bar	H_2/CO_2 ratio	Diameter / cm	Length / cm
10	1	1,07	10

The literature followed focused on comparing different temperature environments with the variation of the inlet amount of CO_2 and H_2, maintaining the feed ratio between them equal to 1. The remain parameters were kept constant.

The obtained results are presented in the following Figure 12. [58]

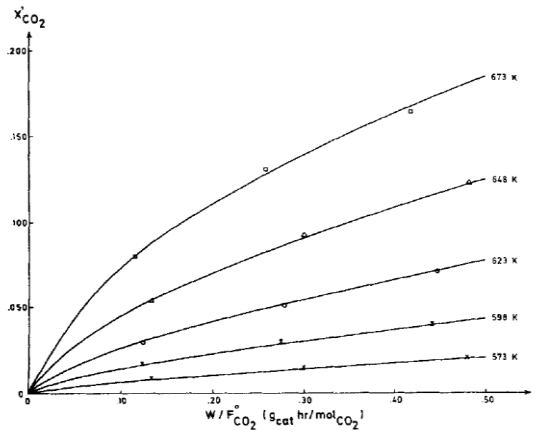

Figure 12. Conversion of CO_2 vs space-time.

A simulation in the same conditions and exact reactor dimensions was performed in Aspen Plus V12 software, to achieve the same rate conversions presented in Figure 12. The reactor, as referred to in the literature, is considered to operate isothermally and at the pressure of 10 bar. The system is then tested for 573, 598, 623, 648 and 673 K.

The simulation environment is represented below in Figure 13.

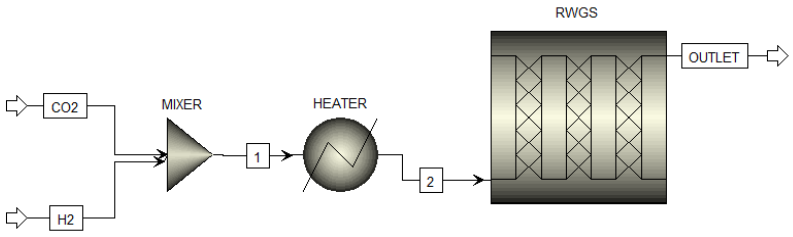

Figure 13. Flowsheet of the process for the validation of the results.

There is feed a stream composition with CO_2 and H_2. As referred, the total flow changes according to the defined ratio W/F_{CO_2}, as presented in the literature.

There was conducted a simulation for each temperature referred, considering the different inlet feed. The conversion values of the simulation results were determined according to the correlation represented in the Eq. 3.14.

$$X_{CO_2} = \frac{f_{CO_2,in} - f_{CO_2,out}}{f_{CO_2,in}} \qquad 3.14$$

The obtained conversions curves and the ones presented in the refereed literature, for each temperature, are displayed in the following Figure 14.

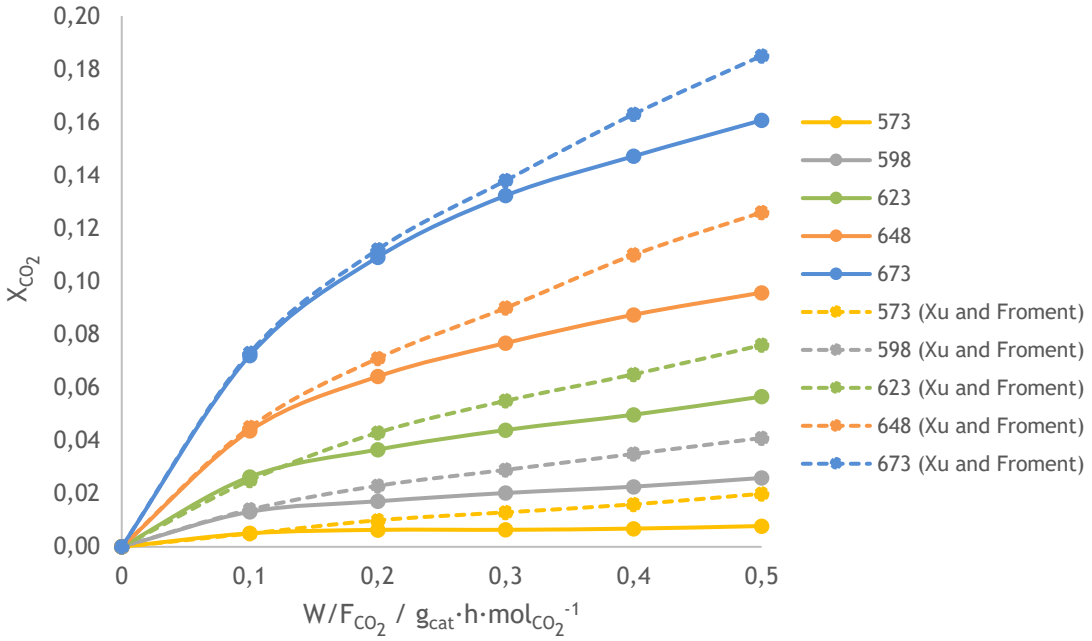

Figure 14. Comparison of the obtained results with the conversions presented in the literature.

Even though the obtained curves do not overlap the literature results, it is observed that for higher inlet flows, the conversions are the same and, mostly, the tendency of conversion growth with the increase of the temperature and the decrease of the inlet flow is respected.

In this case, for the production of 50 L per day of kerosene, the inlet amounts will be inserted between the gap of 0 and 0.1 of the W/F_{CO_2} ratio. This way, the simulation will be conducted in the first section of the previous graph. So, it is possible to guarantee that the obtained results will respect the data in the literature.

It is essential to notice, by Figure 14, that for a higher W/F_{CO_2} ratio, which implies smaller inlets for the same amount of catalyst, the conversion is higher. As expected, when it is fed a smaller amount of the reactants for the same mass of catalyst, the competition to find an active site on the catalyst will be less significant, improving the reaction.

4 Results and Discussion

4.1 Reactions Extent Analysis

To understand the extent of the possible reactions, it was conducted in Aspen Plus V12 software a simulation using a stoichiometric reactor (*Rstoic*). This is characterized as a simple reactor and only requires stoichiometry and the reactions equilibrium conversion as input. The equilibrium conversion is defined as the maximum conversion that one reaction can achieve, at a given temperature and pressure conditions.

To obtain the equilibrium conversions for each reaction, X_j, it was resorted to the solver tool in the Excel program to determine it according to the equilibrium, based on the correlation presented in Eq. 4.1.

$$X_j = -\frac{\upsilon_i \xi_j}{f_{i,in}} \qquad 4.1$$

Where υ_i is the stoichiometric coefficient of the reference component, ξ_j is the extent of the reaction and $f_{i,in}$ the inlet flow of the reference component.

The intermediate steps to determine the equilibrium conversions are presented in Appendix E.

On the other hand, the equilibrium constant, K_j, can be described according to the previous expression given by Eq. 3.9, depending on the temperature.

This equation allows the direct determination of the equilibrium constant of a specific reaction, at a defined temperature operation, in kelvin. For the reactions involved in the studied process to produce syngas, the parameters λ from the literature used for each reaction are summarized in Table 7. [59]

Table 7. Equilibrium coefficient temperature dependency constants.

	λ_1	λ_2	λ_3
1. rWGS	-191 928.1	-3 937.4	3.8143
2. CO_2 Methanation	-730 726.0	24 125.3	-26.9616
3. CO Methanation	-538 798.1	28 062.7	-30.7759
4. Bosch	-121 003.4	16 573.0	-17.3858
5. Boudouard	70 924.7	20 510.4	-21.2000

The solver tool was programmed to obtain the extent results, respecting the equality between the equilibrium constants determined by Eq. 3.9 and the next Eq. 4.2.

$$K_{eq} = P^{\sum \upsilon_i} \prod x_i^{\upsilon_i} \qquad 4.2$$

This convergence allows the obtention of the ξ_j for each reaction and, according to Eq. 4.1, the respective equilibrium conversions. The obtained equilibrium conversions for the temperature of 700 °C, are listed in the next Table 8.

Table 8. Equilibrium conversions of the reactions involved in the process.

Reaction	Conversion / %
rWGS	37.29
CO_2 Methanation	26.13
CO Methanation	18.35
Bosch	7.69
Boudouard	2.29

The reactor was programmed to operate at the same conditions as the rWGS process: 700 °C and 24 bar. The simulation environment is presented in the following Figure 15.

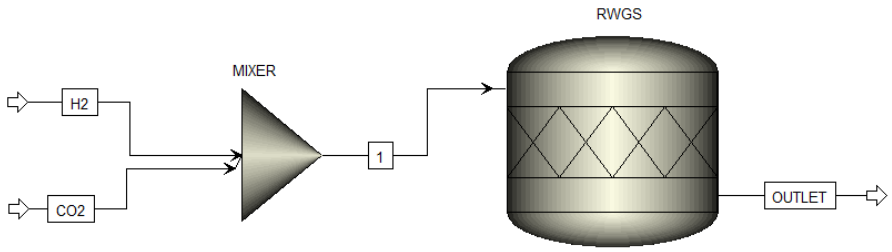

Figure 15. Simulation PFD for the RStoic reactor.

The obtained results are shown in the following Table 9.

Table 9. Extension of the involved reactions.

Reaction	Extension / kmol·h^{-1}
rWGS	0.0552852
CO_2 Methanation	0.0242886
CO Methanation	0.0101448
Bosch	0.0052792
Boudouard	0.0005157

Analysing the results obtained with the simulation, it is possible to conclude that both Bosch and Boudouard reactions can be neglectable in this process, as their extents are less significant, comparing with the remaining. Besides, it is essential to point out that the rWGS is the main reaction, as desired and expectable.

According, according to the extension results, only the rWGS, both CO_2 and CO methanation and the respective reverse reactions will be considered for this study.

4.2 Aspen Simulation

The validated kinetic model developed by Xu and Froment was applied to the simulation that aims at the production of CO to integrate the Fischer-Tropsch process for the production of biokerosene.

Owing to the target production of 50 L per day of biokerosene, the inlet amount of CO_2 and H_2 was determined considering an average conversion of 60% for the Fischer-Tropsch process. [24] Therefore, the production of CO has to offset the 60% conversion. The inlet flows are determined considering that the kerosene obtained is represented by $C_{12}H_{26}$, and so, according to Eq. 2.1, there are necessary 12 molecules of CO to produce one molecule of $C_{12}H_{26}$. The average rWGS conversion for the estimation of the inlet flows is considered to be 40%.

The inlet stream flows determined according to the previous assumption are presented in Table 10.

Table 10. CO_2 and H_2 calculated inlet flows.

Compound	Molar Flow / $kmol \cdot h^{-1}$
CO_2	0.00440572
H_2	0.01321716

It is important to notice that the diesel fraction produced in the Fischer-Tropsch reactor, expected to be large, can be converted into biokerosene through a hydrocracking process. This way, with the addition of H_2, the carbon chain between 16 and 20 carbon molecules can be broken and transformed into biokerosene. However, as this further step is not studied at all in this project, this presumable fraction of kerosene is not considered for the target of 50 L per day.

The results obtained in the simulation are represented in Figure 16.

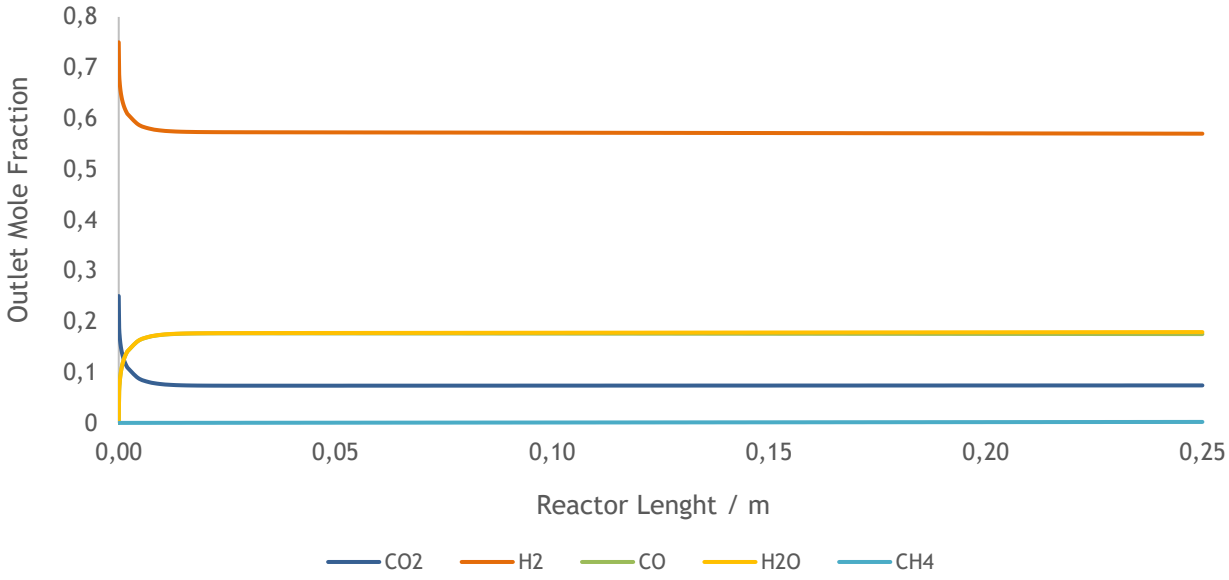

Figure 16. rWGS reactor outlet composition with calculated inlet flows.

Even though the estimated parameters may give a good approximation for the inlet flows, as the present system has complex kinetics, the production of CO by the rWGS reactor is around 0.003073 kmol·h^{-1}, which is equivalent to nearly 80 L·day^{-1} of kerosene at the end of the FT reactor, considering once again the previous assumptions.

The H_2 and CO_2 were then adjusted, resorting to the program Aspen Plus V12, to accomplish the desire production of 50 L·day^{-1} of kerosene. The adjusted values are represented in Table 11.

Table 11. CO_2 and H_2 adjusted inlet flows.

Compound	Molar Flow / kmol·h^{-1}
CO_2	0.00279196
H_2	0.00837589

4.2.1 Catalyst Weight

In order to understand the mass of catalyst that should be used to achieve the target of CO, it was performed a sensitivity analysis. The conditions applied are the ones chosen to operate this process: 973 K and 24 bar. The reactor dimensions used are the ones referred to in the reference literature. The mass of catalyst is also the one referred in the Xu and Froment experiments, 0.0004 kg.

The sensitivity analysis is represented in Figure 17.

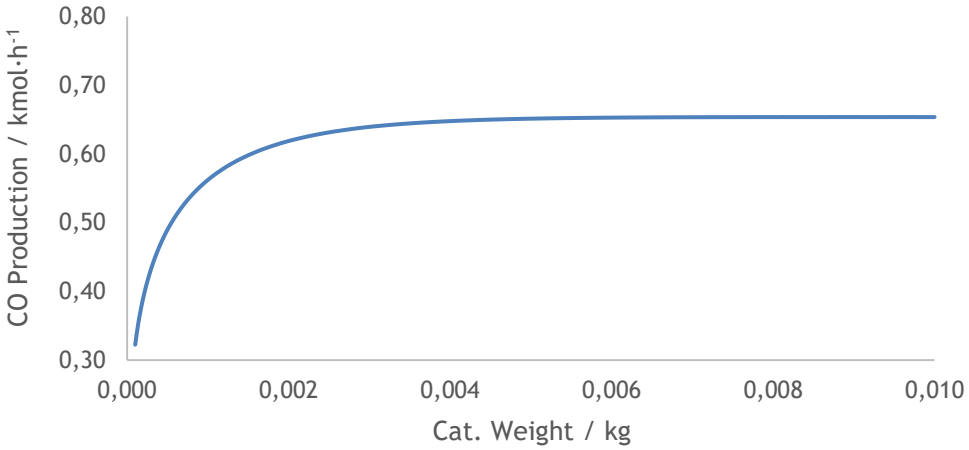

Figure 17. Sensitivity analysis to the mass of the catalyst.

The sensibility analyses to the mass of catalyst allow us to understand how it influences the outlet flow of CO. It is possible to observe that beyond 0.006 kg of catalyst, the outlet flow does not change with the increase of the catalyst inside the reactor. According to this analysis, this study should be used 0.006 kg of catalyst.

Knowing the mass of catalyst needed, it is possible to determine the reactor volume to support this process. With the density of the catalyst of 1870 $kg \cdot m^{-3}$, the catalyst volume can be established. [60] Using Eq. 4.3, the volume of the reactor occupied by the catalyst can be determined, considering a bed porosity, ε_b, of 0.4.

$$V_{reactor} = \frac{V_{catalyst}}{(1 - \varepsilon_b)} \qquad 4.3$$

As referred to in Chapter 2.3.5, the catalyst is diluted with alumina to control the temperature and prevent runaway or damage of the catalyst. Respecting then the ratio applied in the literature, for this study, the catalyst is diluted in 1.3×10^{-4} m^3 of alumina.

As a result of the previous volumes, the total volume of the reactor determined is to be 0.000135 m^3.

Assuming that this reactor respects the ratio between the length and the diameter of the reference reactor ($L/D_{Xu\ and\ Froment} = 9.35$) and is designed according to the standard ratio, between 5 and 10, the dimensions of the desired reactor will be the ones described in the following Table 12.

Table 12. Reactor dimensions.

Length / m	Diameter / m
0.25	0.026

The temperature, as explained in Chapter 2.3.1, is 973 K, and the pressure of the process is 24 bar. The CO_2 and H_2 streams were considered pure in order to simplify the calculations and to keep the process as simple as possible in this first approach.

In Figure 18, there is represented the simulation flowsheet in the program Aspen Plus V12.

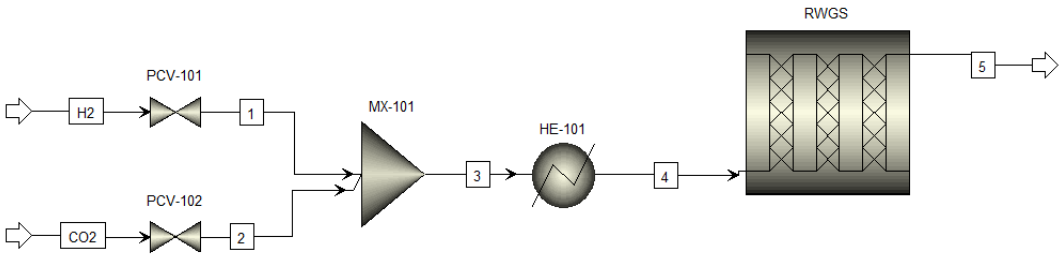

Figure 18. rWGS simulation PFD.

The results obtained are represented graphically in Figure 19.

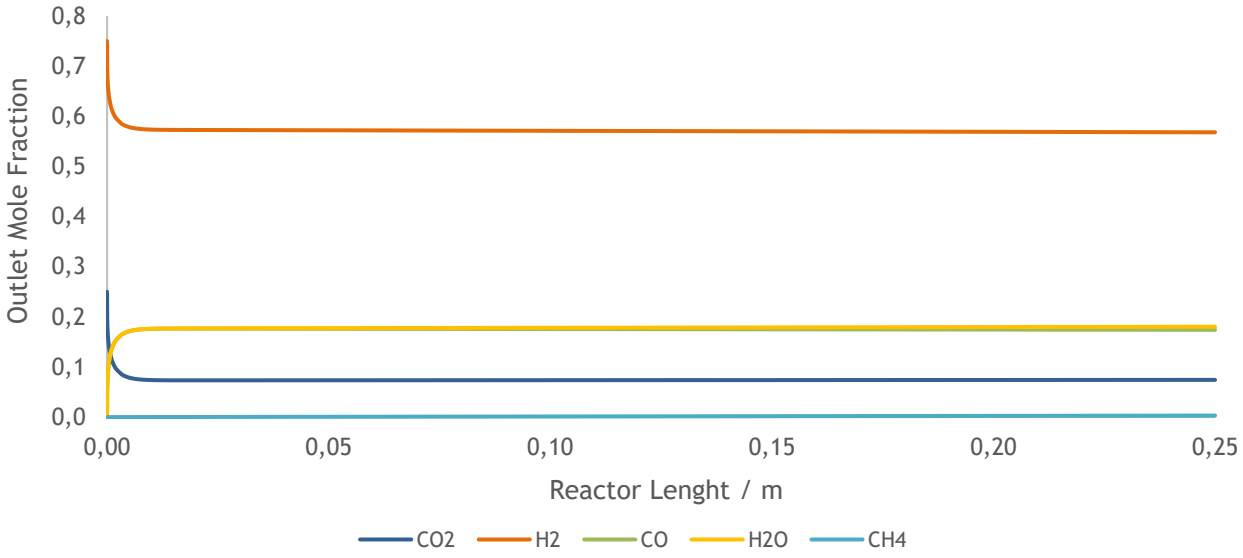

Figure 19. rWGS reactor outlet composition with adjusted inlet flows.

The production of CO happens relatively fast, as expected. The rWGS reaction, responsible for the CO production, is controlled by the kinetic and, as referred to in Chapter 3.1, it is almost instantaneous.

Even though the production of CH_4 is nearly inexistent, according to Figure 19, there is a fraction of methane in the final stream.

Another important piece of information observed in Figure 19 is the subsequent production of CH_4 and the adjacent consumption of CO, described by the CO methanation reaction. Also, CO_2 and H_2 are continuously consumed for the production of CH_4, according to the CO_2 methanation

reaction. In Figure 20, it is possible to observe, on an enlarged scale, the importance of the methanation reactions on the consumption of CO and the production of CH_4.

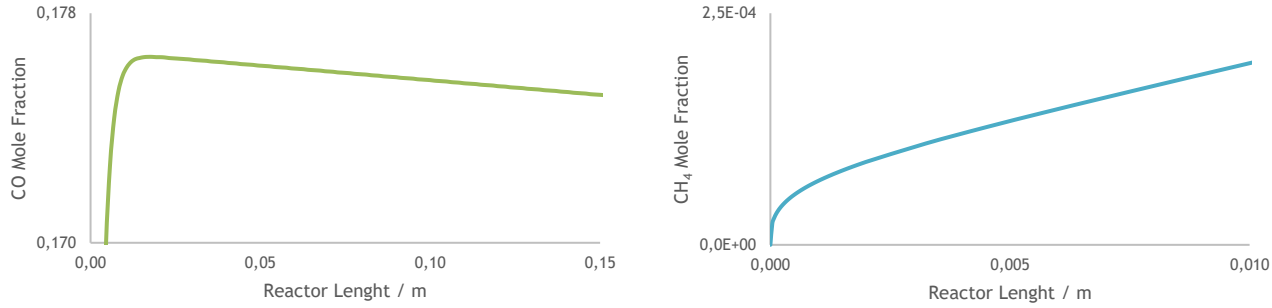

Figure 20. a) CO consumption and b) CH_4 formation.

The solution for the optimization of this data might be the reduction of the residence time. As referred to in Chapter 2.3.3, the residence time for the rWGS reaction is between 5 and 64 ms and the program determined a residence time of 5.09 s. This information reveals that the reactants and the products are residing more than enough time referenced for the rWGS, which leads to side reactions, such as the CO_2 and CO methanation, which have slower kinetics. Consequently, increase the residence time inside the reactor beyond the referenced time for the rWGS reaction allows the formation of CH_4 and therefore the consumption of CO takes place, as verified.

4.2.2 Optimization of the reactor

With the aim to lower the production of CH_4, it was introduced an inert carrier (N_2) in the process.

The inert has an essential role in increasing the volume per time entering in the reactor, which leads to the decrease of the residence time since the reactor volume is fixed and constant. [28] Also, operating with the feed diluted in the inert helps to reduce temperature gradients in the catalytic bed, as explained in Chapter 2.3.6. [34]

In Figure 21, there is represented the PFD with the addition of the N_2 stream.

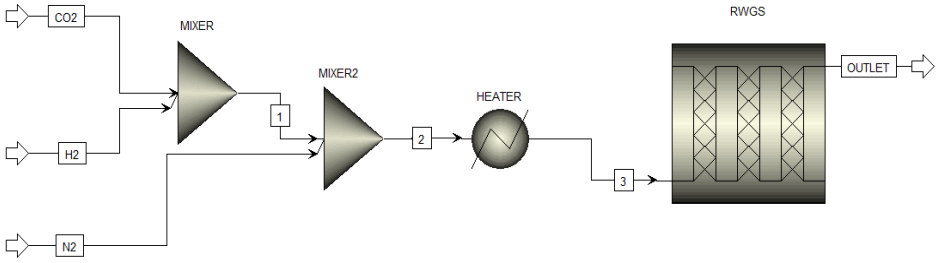

Figure 21. PFD with the inert stream.

A sensitivity analysis to the residence time was conducted in the program Aspen Plus V12 to understand if the inert stream influences the expected results. The obtained results are presented in Figure 22.

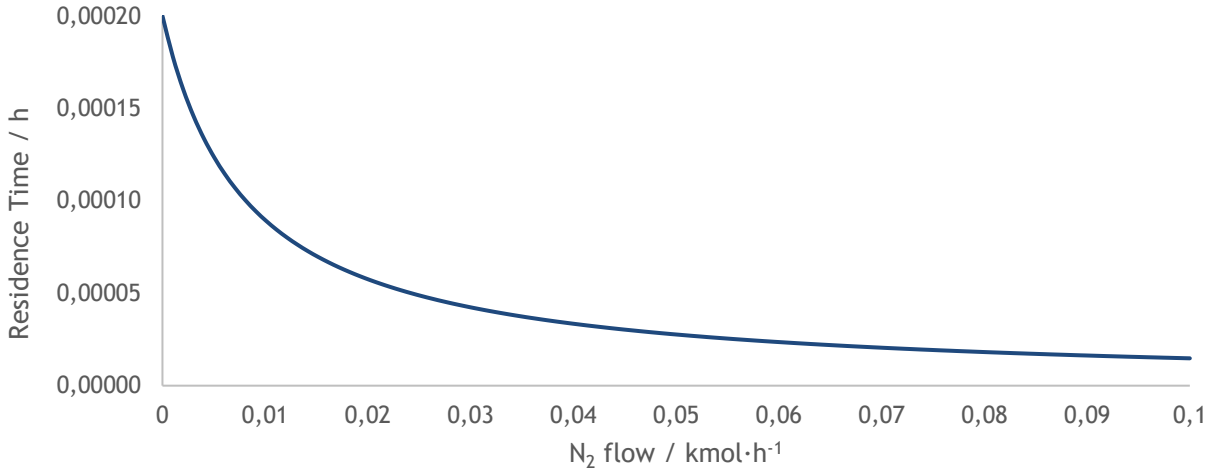

Figure 22. Residence time sensitivity analysis.

As expected initially and according to the literature information, as the inert flow increases the residence time drops significantly. The influence of the inert stream in the production of CO and CH_4 in represented in Figure 23.

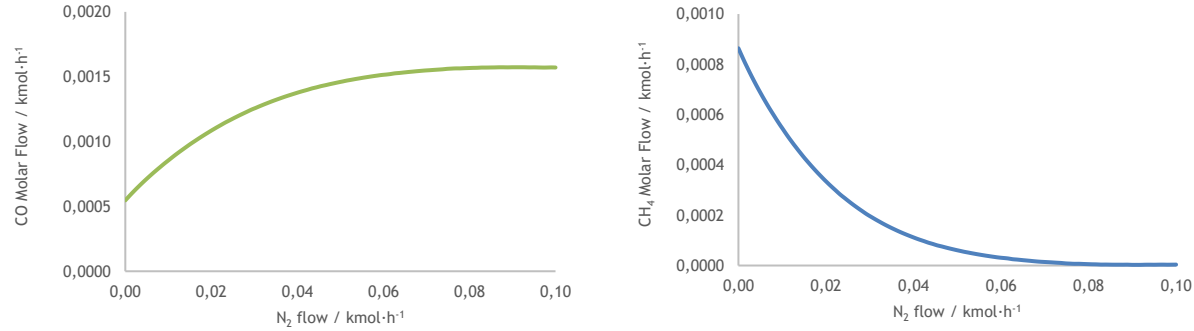

Figure 23. a) CO and b) CH_4 production sensitivity analysis.

As it is possible to observe, with the increase of the N_2 inlet ratio, as the residence time decreases, the production of CH_4 is suppressed, and the final amount of CO is higher since it is not being consumed for the CO methanation reaction.

To optimize the CO production in the rWGS process, there was introduced an N_2 stream to the process, as represented in Figure 21. According to the sensitivity analysis to the CO and CH_4 production, the maximum and minimum point, respectively, are achieved when the N_2 inlet flow is around 0.09 $kmol \cdot h^{-1}$, which will be selected as the amount fed into the process.

The difference between the consumption of CO and the production of CH_4 with and without the introduction of the N_2 stream is significant and the graphs that allow this comparison is represented in Figure 24.

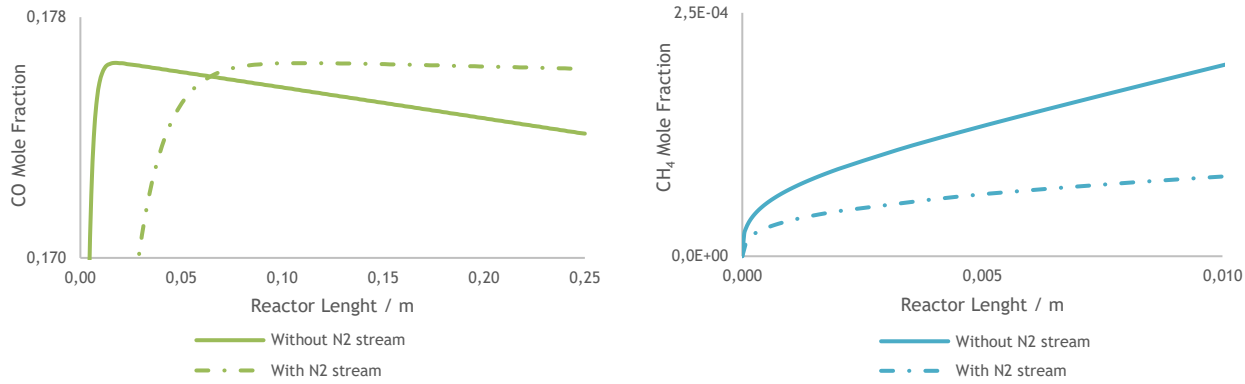

Figure 24. Comparison of the a) CO consumption and b) CH_4 formation with the introduction of the N_2 flow.

The dashed lines describe the CO consumption and the production of CH_4 with the introduction of the inert stream, comparing with the curves represented previously in Figure 20. As predicted, and possible to check by the graphs represented in Figure 24, when added the inert stream, as the residence time decreases, the methanation reactions are suppressed and, consequently, the production of CH_4 and the consumption of CO are minimized.

4.2.3 Water removal

After the rWGS reactor, the outlet stream, composed by non-reacted CO_2 and H_2, CO, CH_4 and H_2O, is fed to the Fischer-Tropsch process for the transformation of CO and H_2 into fuel gases, including biokerosene.

According to Le Chatelier Principle, the presence of water in the Fischer-Tropsch reactor deflects the equilibrium towards the production CO. It suppresses the production of hydrocarbons, as is possible to observe in Eq. 2.1, 2.2 and 2.3.

On the other hand, according to Eq. 2.4, the presence of CO_2 in the process, and as the H_2 is feed in excess into the reactor, even though leads to the production of CO, also leads to the production of H_2O, which is not desirable to the process. All the CO production must be completed in the rWGS step and the water must be removed before the FT synthesis.

The water may be easily removed by condensation, resorting to a condensation vessel and decreasing the temperature to the saturation temperature at the operating pressure. Even though the pressure in the vessel is 24 bar, for the removal of the water it must consider the partial pressure of the water, which is obtained by the multiplication of the molar fraction of the water in the vessel by the total pressure, as follow in the Eq. 4.4.

$$p_i = x_i P \qquad 4.4$$

Where x_i represents the molar fraction of the water and P the total pressure. Attending that the molar fraction of the water in the stream is 0.1804, the partial pressure of the water in the vessel will be 4.34 bar.

For the determined partial pressure, the saturation temperature of the water can be obtained by interpolation of two points from the water thermodynamic tables present in Annex B. Therefore, the saturation temperature of the water in this study is 419.61 K.

This simulation for the water removal was performed in the program Aspen Plus V12. The PFD is represented next in Figure 25.

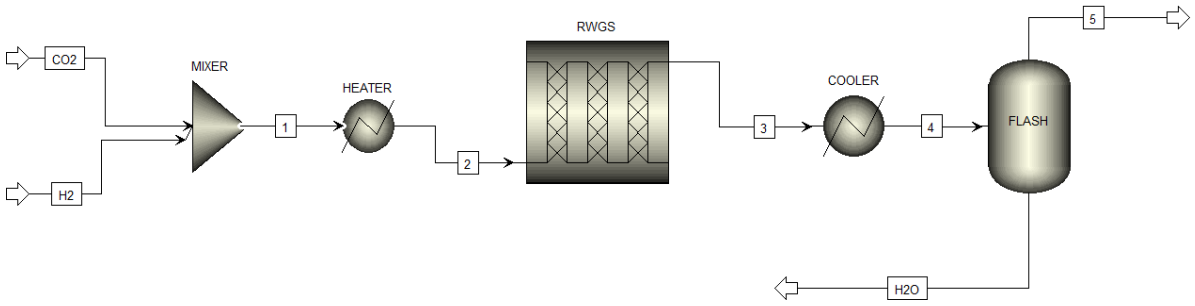

Figure 25. Water removal PFD.

It is expected that, operating the condensation vessel at the exact saturation temperature, the separation will not be efficient. Hence, the partition splits less than 2% of the inlet water.

Resorting to the Aspen Plus V12 function *design spec*, it possible to determine the saturation temperature required for the desired separation. Thus, considering that the desire separation is to obtain the maximum water flow at the H_2O stream, the temperature determined by the software for the flash is 309.83 K.

Applying the temperature determined, the achieved water separation is now near 99%, with a composition of approximately 97% of the water in the bottom stream.

The molar fraction composition of the H_2O stream is represented in Figure 26.

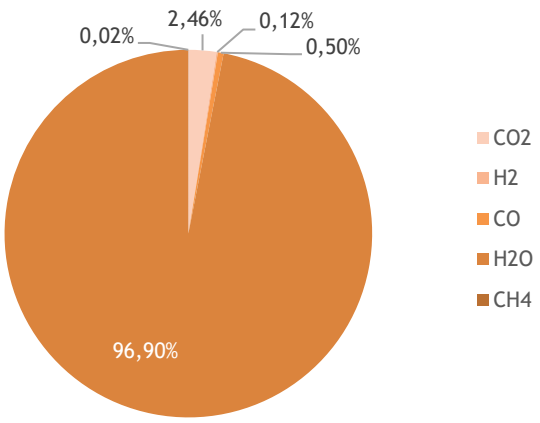

Figure 26. Molar fraction composition of the H_2O stream.

The presence of other components in the water stream, even though the saturation point of the compounds is lower than the 309.83 K, is expectable, as they easily dissolve in water, especially the CO_2, as its solubility in water is relatively high. According to the literature, the solubility, especially of the CO_2 and the CO molecules, is significant, which justifies the major presence of these compounds in the H_2O stream. [61]

Table 13 presents the solubility of the residual compounds presented in the condensation vessel bottom stream.

Table 13. Compounds solubility at 309,81 K.

Compound	Solubility / $g_{gas} \cdot kg_{water}^{-1}$
CO_2	1.0000
CO	0.0210
CH_4	0.0160
H_2	0.0014

The graphs that characterize the solubility of the compounds according to the temperature are presented in Annex C.

5 Conclusion

It is known that mankind's activities have been leading to uncontrolled pollution levels, so new solutions and technology to suppress it should be implemented. This work was focus on the aircraft sector and an alternative to produce biokerosene through CO_2. This solution might represent a huge step for the aviation sector due to the recycling of already existing CO_2, besides the kerosene production in a sustainable way.

This work studied and selected Xu and Froment's model to represent the rWGS process and the reactions involved. With the reproduction of the test made by the authors in the program Aspen Plus V12, it was possible to conclude that, even though the obtained curves do not overlap, in the available range of values, the maximum deviation to the authors results is 5,88%. It was assumed that the model would represent the current reactive system and the results obtained with the Aspen Plus V12 program would be given according to Xu and Froment's model.

Starting with Xu and Froment's experiments, the inlet flows were adjusted to the desired biokerosene flow of 50 $L \cdot day^{-1}$ and a new simulation was run. To understand the ideal mass of catalyst for this process, it was conducted a sensitivity analysis and the mass of 0.006 kg of the catalyst was concluded to be ideal.

The volume of the reactor was determined considering the mass of the catalyst required and the volume of alumina needed to add, not only control runaways, but also to dilute the catalyst and distribute it along the catalytic bed. The volume was determined to be $1.35 \times 10^{-4}\ m^3$. To maintain the same relation between the length and the reactor diameter applied in Xu and Froment's model, it was concluded that the reactor would have a 0.25 m length and a diameter of 0.026 m.

Even though the residual production of CH_4 in this scenario, $3.46 \times 10^{-5}\ kmol \cdot h^{-1}$, this value can be optimized with the introduction of the inert stream to reduce the residence time. In the literature, it is referred that for the rWGS process, the residence time should be smaller than 64 ms to give place for the rWGS only, as the methanation reactions have a longer residence time. In this case, the residence time is 5.09 s.

With the introduction of the N_2 stream, it was possible to reduce the residence time to 58.74 ms and to have a decrease of 82.25% in the production of CH_4 along the process. Even though the production of CH_4 is already residual, it is essential to reduce it as much as possible, especially due to the consumption of CO to produce CH_4, through the CO methanation reaction.

Finally, it was simulated a water removal unit since water is highly unwanted in the FT process and has to be removed. To accomplish this unit, it was considered the partial pressure of the water and the respective saturation temperature. As the separation at the saturation temperature was not completed, it was resorted the tool *design spec* in Aspen Plus V12 software to determine the ideal temperature of 309.83 K. The water was successfully separated from the other compounds, but due to the solubilities, it was not possible to avoid the dragging of essentially CO_2 and CO.

At this point, it is possible to send the stream to the FT reactor. Still, it is suggested to accomplish the CH_4 and CO_2 removal and recycling, respectively, after the rWGS reactor, both with membranes utilization. I leave these points as suggestions for future works on this topic.

In the future, it should be considered a study to understand the solubility of the compounds in the water and their influence on the process.

In order to keep up with the latest advances, it should be studied the implementation of a membrane reactor, to minimize the complexity of the process and to run in a single reactor both rWGS and FT reactions.

As an overview, it is possible to affirm that the objectives proposed were achieved and the realization of this work allows a good starting point for DMT Environmental Technology to have a relevant presence in the biofuels market.

Finally, it is essential to underline the growing effort by airlines to decrease CO_2 emissions. The investment in sustainable aviation knowledge and technology is a trend to provide solutions to face this environmental problem.

Undeniably, there are still lacks in this area, especially the mature technology available. Even though, renewable jet fuel is a potential short-term solution to reduce the pollution levels and hence decrease the climate impact of flying. To make this breakthrough possible, governmental financial support mechanisms are required for industries and aviation companies to invest in this solution and cover the difference in the costs between ordinary fossil fuels and renewable jet fuels.

6 Assessment of the work done

6.1 Objectives Achieved

The objectives of this project consisted in the design of a reactor to produce syngas over CO_2 and H_2, obtained from renewable sources. In order to achieve the proposed objectives, it was accomplished:

- The study and selection of the kinetic model to describe the reactions involved
- The validation of Xu and Froment's model
- Application of the model and acquirement of the results
- Optimization of the results by adding the inert stream
- Removal of the water with the condensation vessel

All the proposed objectives at the beginning of this project were achieved.

6.2 Final Assessment

This project regarding the design of a reactor to produce CO over CO_2 and H_2 was found challenging and extremely enriching from an academic point of view. The general knowledge reached in this last six months project is also significant and a starting point for the company goals.

Even though there is good work done on this topic, there is still a lot to do, starting with the design of the remain units, especially the FT reactor and the upgrading unit, to optimize the final product and, possibly, to transform the diesel fraction obtained into kerosene though a hydrocracking process.

After all, the objective of the company is to be present in the aviation market and to compete with companies already installed in the fuels field. For that, a scale-up of all the units as also to be consider in order to be able to be competitive in this area.

7 References

[1] Song C. Global challenges and strategies for control, conversion and utilization of CO2 for sustainable development involving energy, catalysis, adsorption and chemical processing. *Catal Today* 2006; 115: 2–32.

[2] Quadrelli R, Peterson S. The energy-climate challenge: Recent trends in CO2 emissions from fuel combustion. *Energy Policy* 2007; 35: 5938–5952.

[3] Chiaramonti D, Prussi M, Buffi M. Sustainable biokerosene: Process routes and industrial demonstration activities in aviation biofuels. *Appl Energy* 2014; 136: 767–774.

[4] Bruce S, Temminghoff M, Hayward J. Opportunities for Hydrogen in Commercial Aviation. *Csiro*.

[5] Linden P Van Der, Office M. Climate Change 2007: Impacts, Adaptation and Vulnerability. *Environ Res Lett*.

[6] Bruhn T, Naims H, Olfe-Kräutlein B. Separating the debate on CO2 utilisation from carbon capture and storage. *Environ Sci Policy* 2016; 60: 38–43.

[7] Aresta M, Tommasi I. Carbon dioxide utilisation in the chemical industry. *Energy Convers Manag* 1997; 38: S373–S378.

[8] Pacheco MA, Marshall CL. Review of dimethyl carbonate (DMC) manufacture and its characteristics as a fuel additive. *Energy and Fuels* 1997; 11: 2–29.

[9] Goldmann A, Sauter W, Oettinger M. A study on electrofuels in aviation. *Energies* 2018; 11: 1–23.

[10] Neuling U, Kaltschmitt M. Conversion routes for production of biokerosene—status and assessment. *Biomass Convers Biorefinery* 2015; 5: 367–385.

[11] Gormley RJ, Link DD, Baltrus JP. Interactions of jet fuels with nitrile o-rings: Petroleum-derived versus synthetic fuels. *Energy and Fuels* 2009; 23: 857–861.

[12] Guell BM, Bugge M, Kempegowda RS. Benchmark of conversion and production technologies for synthetic biofuels for aviation. *Sintef* 2012; 95.

[13] Brooks KP, Snowden-Swan LJ, Jones SB. *Low-Carbon Aviation Fuel Through the Alcohol to Jet Pathway*. Elsevier Inc. Epub ahead of print 2016. DOI: 10.1016/b978-0-12-804568-8.00006-8.

[14] Duong LH, Reksowardojo IK, Soerawidjaja TH. Soap-derived biokerosene as an aviation alternative fuel: Production, composition, and properties of various blends with jet fuel.

Chem Eng Process - Process Intensif 2020; 153: 107980.

[15] van der Laan GP. *Kinetics, Selectivity and Scale-Up of the Fischer-Tropsch Synthesis*. 1999.

[16] Kaltschmitt M, Neuling U. *Biokerosene: status and prospects*. 2018.

[17] Saeidi S, Nikoo MK, Mirvakili A. Recent advances in reactors for low-temperature Fischer-Tropsch synthesis: Process intensification perspective. *Rev Chem Eng* 2015; 31: 209–238.

[18] Tijmensen MJA, Faaij APC, Hamelinck CN. Exploration of the possibilities for production of Fischer Tropsch liquids and power via biomass gasification. *Biomass and Bioenergy* 2002; 23: 129–152.

[19] Klerk A De. Fischer-Tropsch fuels refinery design. *Energy Environ Sci* 2011; 4: 1177–1205.

[20] Steynberg AP, Dry ME, Davis BH. *Fischer-Tropsch reactors*. Elsevier B.V. Epub ahead of print 2004. DOI: 10.1016/s0167-2991(04)80459-2.

[21] Guettel R, Kunz U, Turek T. Reactors for Fischer-Tropsch synthesis. *Chem Eng Technol* 2008; 31: 746–754.

[22] de Deugd RM. *Fischer-Tropsch Synthesis Revisited; Efficiency and Selectivity Benefits from Imposing Temporal and/or Spatial Structure in the Reactor*. 2004.

[23] Hamelinck CN, Faaij APC. Outlook for advanced biofuels. *Energy Policy* 2006; 34: 3268–3283.

[24] Van de Loosdrecht J, Botes FG, Ciobica IM. *Fischer-Tropsch Synthesis: Catalysts and Chemistry*. Elsevier Ltd. Epub ahead of print 2013. DOI: 10.1016/B978-0-08-097774-4.00729-4.

[25] Leigh GJ. *Catalysis in C1 Chemistry*. 1984. Epub ahead of print 1984. DOI: 10.1016/0022-328x(84)80151-5.

[26] Rohde MP, Unruh D, Schaub G. Membrane application in Fischer-Tropsch synthesis reactors - Overview of concepts. *Catal Today* 2005; 106: 143–148.

[27] Liuzzi D, Fernandez E, Perez S. Advances in membranes and membrane reactors for the Fischer-Tropsch synthesis process for biofuel production. *Rev Chem Eng*. Epub ahead of print 3 April 2020. DOI: 10.1515/revce-2019-0067.

[28] Daza YA, Kuhn JN. CO2 conversion by reverse water gas shift catalysis: Comparison of catalysts, mechanisms and their consequences for CO2 conversion to liquid fuels. *RSC Adv* 2016; 6: 49675–49691.

[29] Mirodatos C, Praliaud H, Primet M. Deactivation of nickel-based catalysts during CO

methanation and disproportionation. *J Catal* 1987; 107: 275–287.

[30] Bartholomew CH. Mechanisms of catalyst deactivation. Epub ahead of print February 2001. DOI: 10.1016/j.cej.2018.09.156.

[31] Wolf A, Jess A, Kern C. Syngas Production via Reverse Water-Gas Shift Reaction over a Ni-Al2O3 Catalyst: Catalyst Stability, Reaction Kinetics, and Modeling. *Chem Eng Technol* 2016; 39: 1040–1048.

[32] Zhang L, Chen L, Xia S. Entropy generation minimization for reverse water gas shift (RWGS) reactors. *Entropy*; 20. Epub ahead of print 2018. DOI: 10.3390/e20060415.

[33] Ghaib K, Nitz K, Ben-Fares F-Z. Chemical Methanation of CO 2 : A Review. *ChemBioEng Rev* 2016; 3: 266–275.

[34] Vidal Vázquez F, Pfeifer P, Lehtonen J. Catalyst Screening and Kinetic Modeling for CO Production by High Pressure and Temperature Reverse Water Gas Shift for Fischer-Tropsch Applications. *Ind Eng Chem Res* 2017; 56: 13262–13272.

[35] Ranjbar A, Irankhah A, Aghamiri SF. Reverse water gas shift reaction and CO2 mitigation: Nanocrystalline MgO as a support for nickel based catalysts. *J Environ Chem Eng* 2018; 6: 4945–4952.

[36] Kwack SH, Park MJ, Bae JW. Development of a kinetic model of the Fischer-Tropsch synthesis reaction with a cobalt-based catalyst. *React Kinet Mech Catal* 2011; 104: 483–502.

[37] Vanderwiel DP, Wang Y, Tonkovich Y. Carbon Dioxide Conversions in Microreactors. 187–193.

[38] Vita A, Cristiano G, Italiano C. Syngas production by methane oxy-steam reforming on Me/CeO2 (Me=Rh, Pt, Ni) catalyst lined on cordierite monoliths. *Appl Catal B Environ* 2015; 162: 551–563.

[39] Ahn SH, Choi I, Kwon OJ. Hydrogen production through the fuel processing of liquefied natural gas with silicon-based micro-reactors. *Chem Eng J* 2014; 247: 9–15.

[40] Sehested J. Four challenges for nickel steam-reforming catalysts. *Catal Today* 2006; 111: 103–110.

[41] Zeppieri M, Villa PL, Verdone N. Kinetic of methane steam reforming reaction over nickel- and rhodium-based catalysts. *Appl Catal A Gen* 2010; 387: 147–154.

[42] Lazar MD, Dan M, Mihet M. Hydrogen production by low temperature methane steam reforming using Ag and Au modified alumina supported nickel catalysts. *Rev Roum Chim* 2011; 56: 637–642.

[43] Rostrup-Nielsen JR. Catalytic Steam Reforming. *Catal Sci Technol* 1984; 5: 1–117.

[44] SUZUKI T. Selective hydrogenation of CO2 to CO in the presence of excess CO on a MoO3/ZnO catalyst?A preliminary attempt to yield an equimolecular mixture of H2 and CO. *Int J Hydrogen Energy* 1995; 20: 823–830.

[45] Twigg M V., Spencer MS. Deactivation of supported copper metal catalysts for hydrogenation reactions. *Appl Catal A Gen* 2001; 212: 161–174.

[46] Ratnasamy C, Wagner J. Water gas shift catalysis. *Catal Rev - Sci Eng* 2009; 51: 325–440.

[47] Lisboa JDS, Santos DCRM, Passos FB. Influence of the addition of promoters to steam reforming catalysts. *Catal Today* 2005; 101: 15–21.

[48] M A, T P, C P. Experimental optimization of catalytic steam reforming of model biogas. *Chem Eng* 2008; 2–6.

[49] Tomishige K, Chen YG, Fujimoto K. Studies on carbon deposition in CO2 reforming of CH4 over nickel-magnesia solid solution catalysts. *J Catal* 1999; 181: 91–103.

[50] Tsipouriari VA, Verykios XE. Carbon and oxygen reaction pathways of CO2 reforming of methane over Ni/La2O3 and Ni/Al2O3 catalysts studied by isotopic tracing techniques. *J Catal* 1999; 187: 85–94.

[51] Wang JB, Tai YL, Dow WP. Study of ceria-supported nickel catalyst and effect of yttria doping on carbon dioxide reforming of methane. *Appl Catal A Gen* 2001; 218: 69–79.

[52] Najari S, Gróf G, Saeidi S. Modeling and optimization of hydrogenation of CO 2 : Estimation of kinetic parameters via Artificial Bee Colony (ABC) and Differential Evolution (DE) algorithms. *Int J Hydrogen Energy* 2019; 44: 4630–4649.

[53] Faure R, Rossignol F, Chartier T. Alumina foam catalyst supports for industrial steam reforming processes. *J Eur Ceram Soc* 2011; 31: 303–312.

[54] Pour AN, Housaindokht MR, Monhemi H. A new LHHW kinetic model for CO2 hydrogenation over an iron catalyst. *Prog React Kinet Mech* 2016; 41: 159–169.

[55] Choi Y, Stenger HG. Water gas shift reaction kinetics and reactor modeling for fuel cell grade hydrogen. *J Power Sources* 2003; 124: 432–439.

[56] Navarro M V., Plou J, López JM. Effect of oxidation-reduction cycles on steam-methane reforming kinetics over a nickel-based catalyst. *Int J Hydrogen Energy* 2019; 44: 12617–12627.

[57] Halabi MH, de Croon MHJM, van der Schaaf J. Modeling and analysis of autothermal reforming of methane to hydrogen in a fixed bed reformer. *Chem Eng J* 2008; 137: 568–

578.

[58] Xu J, Froment GF. Methane steam reforming, methanation and water-gas shift: I. Intrinsic kinetics. *AIChE J* 1989; 35: 88–96.

[59] Swickrath MJ, Anderson M. The development of models for carbon dioxide reduction technologies for spacecraft air revitalization. *42nd Int Conf Environ Syst 2012, ICES 2012* 2012; 1–19.

[60] de Smet CRH, de Croon MHJM, Berger RJ. Design of adiabatic fixed-bed reactors for the partial oxidation of methane to synthesis gas. Application to production of methanol and hydrogen-for-fuel-cells. *Chem Eng Sci* 2001; 56: 4849–4861.

[61] Sander R. Compilation of Henry's law constants (version 4.0) for water as solvent. *Atmos Chem Phys* 2015; 15: 4399–4981.

[62] Medrano-García JD, Ruiz-Femenia R, Caballero JA. Multi-objective optimization of combined synthesis gas reforming technologies. *J CO2 Util* 2017; 22: 355–373.

[63] Cuijpers E. Ready for a Green Take-Off, https://blog.yieldr.com/airline- (2019).

Annex A – Biokerosene Production Routes

7.1.1 Hydrogenated Ester and Fatty Acids Synthetic Paraffinic Kerosene (HEFA-SPK)

This process is responsible for a 50% maximum blending ratio by volume and consists in the reaction of the feedstock, mainly biomass, vegetable oils and fats or recycled oils, in the presence of H_2 and a catalyst. The process is divided into four main steps: pre-treatment of the feedstock, hydrogenation, isomerization and catalytic cracker and finally the separation of the obtained products. The PFD is described in Figure 27. [16]

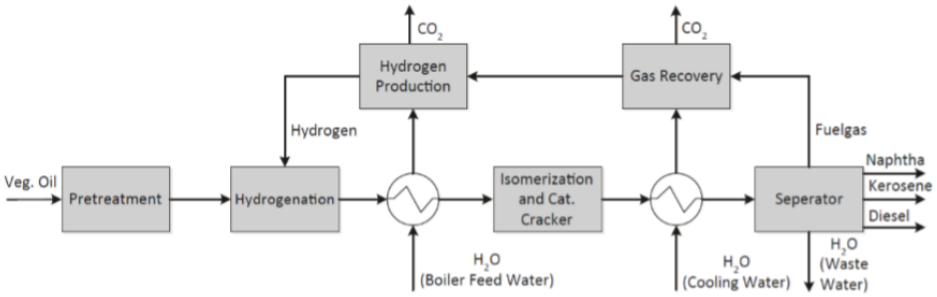

Figure 27. HEFA PFD.

So far, this is the only pathway industrially implanted and so, all the biokerosene produced and commercialized is obtained via HEFA. [62]

However, this pathway requires high amounts of hydrogen, therefore it might not be the most sustainable option for the biokerosene synthesis.

7.1.2 Alcohol to Jet Synthetic Paraffinic Kerosene (AtJ-SPK)

This pathway consists in a biochemical reaction based on the catalytic conversion of methanol, ethanol or butanol, produced by sugar materials (starch-bearing plants and lignocellulosic biomass) into biokerosene.

The well-known route to produce AtJ-SPK biofuel begins with the dehydration of the alcohols. After obtaining alkenes, the process moves to oligomerization, in order to transform them into longer chain hydrocarbons. The last step consists in the distillation of the obtained stream to separate the three products: naphtha, kerosene and diesel.

The process is summarized in Figure 28. [16]

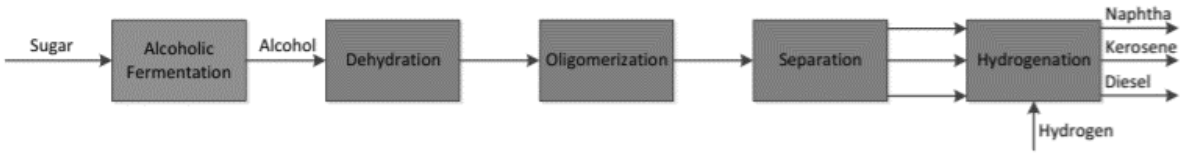

Figure 28. PFD of direct oligomerization of ethylene.

Due to the presence of more challenging process, such as oligomerization, the costs of the AtJ-SPK are expected to be larger, comparing with the HEFA-SPK. [10] Moreover, the availability or price of the feedstock is not an advantage, since it is the same that is used in the previous conversion route.

7.1.3 Direct Sugar to Hydrocarbons (DSHC)

This is a microbial conversion process responsible for the production of synthetic fuel named Synthesized Iso-Paraffins (SIP).

DSHC process requires special pressure and temperature conditions for aerobic fermentation and specific enzymes. Thus, is presented as a complex process and especially complicated to scale up.

In Figure 29, it is represented the DSHC process PFD. [16]

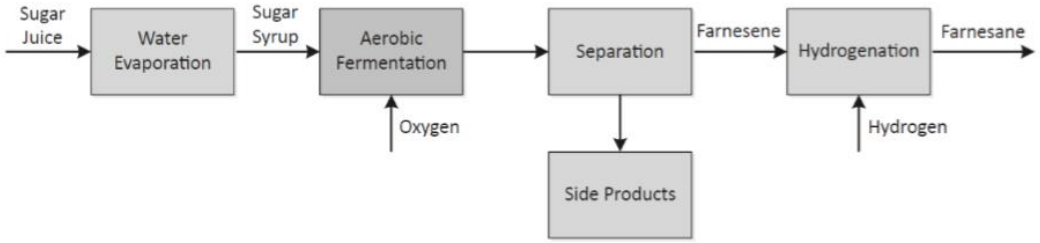

Figure 29. DSHC PFD.

Currently, AtJ, HEFA and FT fuels are already approved by ASTM. [63]

Annex B - Thermodynamic Tables

Table 14. Saturated water properties.

		Specific volume m^3/kg		Internal energy kJ/kg			Enthalpy kJ/kg			Entropy kJ/(kg · K)		
Press. kPa P	Sat. temp. °C T_{sat}	Sat. liquid v_f	Sat. vapor v_g	Sat. liquid u_f	Evap. u_{fg}	Sat. vapor u_g	Sat. liquid h_f	Evap. h_{fg}	Sat. vapor h_g	Sat. liquid s_f	Evap. s_{fg}	Sat. vapor s_g
0.6113	0.01	0.001 000	206.14	0.00	2375.3	2375.3	0.01	2501.3	2501.4	0.0000	9.1562	9.1562
1.0	6.98	0.001 000	129.21	29.30	2355.7	2385.0	29.30	2484.9	2514.2	0.1059	8.8697	8.9756
1.5	13.03	0.001 001	87.98	54.71	2338.6	2393.3	54.71	2470.6	2525.3	0.1957	8.6322	8.8279
2.0	17.50	0.001 001	67.00	73.48	2326.0	2399.5	73.48	2460.0	2533.5	0.2607	8.4629	8.7237
2.5	21.08	0.001 002	54.25	88.48	2315.9	2404.4	88.49	2451.6	2540.0	0.3120	8.3311	8.6432
3.0	24.08	0.001 003	45.67	101.04	2307.5	2408.5	101.05	2444.5	2545.5	0.3545	8.2231	8.5776
4.0	28.96	0.001 004	34.80	121.45	2293.7	2415.2	121.46	2432.9	2554.4	0.4226	8.0520	8.4746
5.0	32.88	0.001 005	28.19	137.81	2282.7	2420.5	137.82	2423.7	2561.5	0.4764	7.9187	8.3951
7.5	40.29	0.001 008	19.24	168.78	2261.7	2430.5	168.79	2406.0	2574.8	0.5764	7.6750	8.2515
10	45.81	0.001 010	14.67	191.82	2246.1	2437.9	191.83	2392.8	2584.7	0.6493	7.5009	8.1502
15	53.97	0.001 014	10.02	225.92	2222.8	2448.7	225.94	2373.1	2599.1	0.7549	7.2536	8.0085
20	60.06	0.001 017	7.649	251.38	2205.4	2456.7	251.40	2358.3	2609.7	0.8320	7.0766	7.9085
25	64.97	0.001 020	6.204	271.90	2191.2	2463.1	271.93	2346.3	2618.2	0.8931	6.9383	7.8314
30	69.10	0.001 022	5.229	289.20	2179.2	2468.4	289.23	2336.1	2625.3	0.9439	6.8247	7.7686
40	75.87	0.001 027	3.993	317.53	2159.5	2477.0	317.58	2319.2	2636.8	1.0259	6.6441	7.6700
50	81.33	0.001 030	3.240	340.44	2143.4	2483.9	340.49	2305.4	2645.9	1.0910	6.5029	7.5939
75	91.78	0.001 037	2.217	384.31	2112.4	2496.7	384.39	2278.6	2663.0	1.2130	6.2434	7.4564
Press. MPa												
0.100	99.63	0.001 043	1.6940	417.36	2088.7	2506.1	417.46	2258.0	2675.5	1.3026	6.0568	7.3594
0.125	105.99	0.001 048	1.3749	444.19	2069.3	2513.5	444.32	2241.0	2685.4	1.3740	5.9104	7.2844
0.150	111.37	0.001 053	1.1593	466.94	2052.7	2519.7	467.11	2226.5	2693.6	1.4336	5.7897	7.2233
0.175	116.06	0.001 057	1.0036	486.80	2038.1	2524.9	486.99	2213.6	2700.6	1.4849	5.6868	7.1717
0.200	120.23	0.001 061	0.8857	504.49	2025.0	2529.5	504.70	2201.9	2706.7	1.5301	5.5970	7.1271
0.225	124.00	0.001 064	0.7933	520.47	2013.1	2533.6	520.72	2191.3	2712.1	1.5706	5.5173	7.0878
0.250	127.44	0.001 067	0.7187	535.10	2002.1	2537.2	535.37	2181.5	2716.9	1.6072	5.4455	7.0527
0.275	130.60	0.001 070	0.6573	548.59	1991.9	2540.5	548.89	2172.4	2721.3	1.6408	5.3801	7.0209
0.300	133.55	0.001 073	0.6058	561.15	1982.4	2543.6	561.47	2163.8	2725.3	1.6718	5.3201	6.9919
0.325	136.30	0.001 076	0.5620	572.90	1973.5	2546.4	573.25	2155.8	2729.0	1.7006	5.2646	6.9652
0.350	138.88	0.001 079	0.5243	583.95	1965.0	2548.9	584.33	2148.1	2732.4	1.7275	5.2130	6.9405
0.375	141.32	0.001 081	0.4914	594.40	1956.9	2551.3	594.81	2140.8	2735.6	1.7528	5.1647	6.9175
0.40	143.63	0.001 084	0.4625	604.31	1949.3	2553.6	604.74	2133.8	2738.6	1.7766	5.1193	6.8959
0.45	147.93	0.001 088	0.4140	622.77	1934.9	2557.6	623.25	2120.7	2743.9	1.8207	5.0359	6.8565
0.50	151.86	0.001 093	0.3749	639.68	1921.6	2561.2	640.23	2108.5	2748.7	1.8607	4.9606	6.8213
0.55	155.48	0.001 097	0.3427	655.32	1909.2	2564.5	665.93	2097.0	2753.0	1.8973	4.8920	6.7893
0.60	158.85	0.001 101	0.3157	669.90	1897.5	2567.4	670.56	2086.3	2756.8	1.9312	4.8288	6.7600
0.65	162.01	0.001 104	0.2927	683.56	1886.5	2570.1	684.28	2076.0	2760.3	1.9627	4.7703	6.7331
0.70	164.97	0.001 108	0.2729	696.44	1876.1	2572.5	697.22	2066.3	2763.5	1.9922	4.7158	6.7080
0.75	167.78	0.001 112	0.2556	708.64	1866.1	2574.7	709.47	2057.0	2766.4	2.0200	4.6647	6.6847
0.80	170.43	0.001 115	0.2404	720.22	1856.6	2576.8	721.11	2048.0	2769.1	2.0462	4.6166	6.6628
0.85	172.96	0.001 118	0.2270	731.27	1847.4	2578.7	732.22	2039.4	2771.6	2.0710	4.5711	6.6421
0.90	175.38	0.001 121	0.2150	741.83	1838.6	2580.5	742.83	2031.1	2773.9	2.0946	4.5280	6.6226
0.95	177.69	0.001 124	0.2042	751.95	1830.2	2582.1	753.02	2023.1	2776.1	2.1172	4.4869	6.6041
1.00	179.91	0.001 127	0.194 44	761.68	1822.0	2583.6	762.81	2015.3	2778.1	2.1387	4.4478	6.5865
1.10	184.09	0.001 133	0.177 53	780.09	1806.3	2586.4	781.34	2000.4	2781.7	2.1792	4.3744	6.5536
1.20	187.99	0.001 139	0.163 33	797.29	1791.5	2588.8	798.65	1986.2	2784.8	2.2166	4.3067	6.5233
1.30	191.64	0.001 144	0.151 25	813.44	1777.5	2591.0	814.93	1972.7	2787.6	2.2515	4.2438	6.4953

Annex C – Solubility vs Temperature

Solubility of CO_2

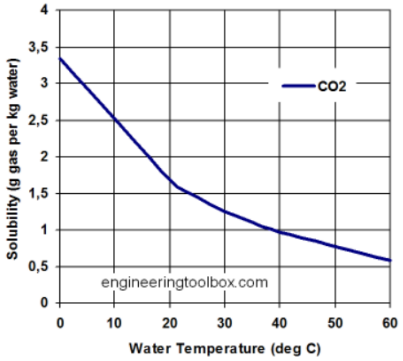

Solubility of CO

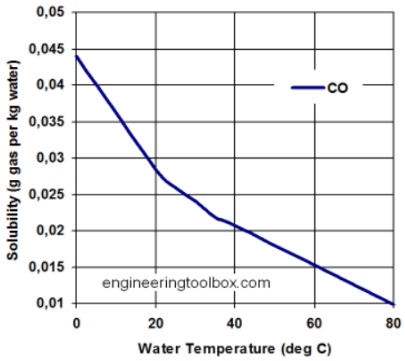

Solubility of CH_4

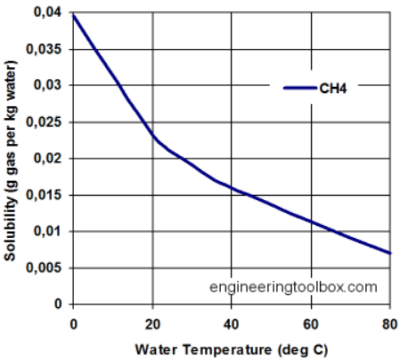

Solubility of H_2

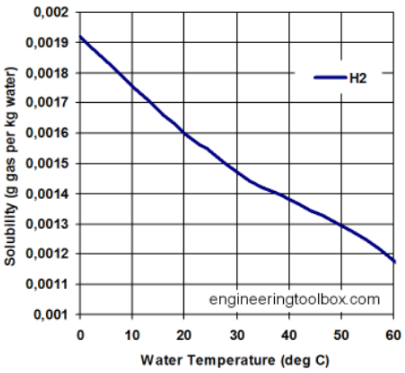

Appendix A - Catalyst House of Quality

Row #	Weight Chart	Relative Weight	Importance (1-5)	Category	Requirements / Technology	Improvement Direction	Cobalt	Iron	Nickel	Ruthenium
1		8%	5	**Product**	Quality	↑	5	3	4	5
2		5%	3		Need of after-treatment	↓	5	4	4	5
3		6%	4	**Poisoning**	Resistance to oxidation	↑	4	3	2	5
4		8%	5		Sintering	↑	4	2	3	5
5		6%	4		Coke formation	↑	5	3	4	4
6		3%	2		Poisoning (sulphur content)	↑	5	3	5	4
7		8%	5		Sensitivity to other contaminants	↑	4	3	4	2
8		8%	5	**Activity**	Fischer-Tropsch	↑	5	3	4	5
9		6%	4		Loss of activity	↓	5	3	4	4
10		8%	5	**Safety**	Thermal stability	↑	3	5	3	5
11		6%	4		Mechanical stability	↑	5	4	3	5
12		8%	5	**Costs**	Price ratio	↓	4	5	3	1
13		6%	4		Lifetime	↑	5	3	1	4
14		8%	5	**Technology**	Availability	↑	5	5	3	1
15		8%	5		Know-how	↑	5	5	4	1
						Target (1-5)	3,0	3,0	3,0	3,0
						Rating	4,55	3,65	3,35	3,63
						Relative Weight	30,0%	24,0%	22,1%	23,9%
						Weight Chart				
						Position	1	2	4	3

Appendix B - Reactor House of Quality

Row #	Weight Chart	Relative Weight	Importance (1-5)	Category	Technology / Requirements	Improvement Direction	MTFB reactor	SB reactor	FB reactor	M reactor
1		6%	5	**Product**	Quality	↑	5	5	1	5
2		6%	5		Products without after-treatment	↑	5	5	1	5
3		6%	5		Capacity	↑	5	4	5	2
4		4%	3		Heat transfer	↑	3	5	5	5
5		1%	1		Mass transfer	↑	3	5	5	5
6		5%	4	**Sustainability**	CO_2 footprint	↓	4	4	3	5
7		5%	4		Energy demand	↓	4	4	3	5
8		4%	3		Catalyst Regeneration	↑	5	3	2	5
9		2%	2		Energy Waste	↓	5	5	4	5
10		5%	4	**Operation**	Downtime	↓	3	5	5	3
11		2%	2		Complexity	↓	4	4	2	3
12		2%	2		Operability	↓	5	5	4	3
13		4%	3	**Safety**	Reactor Conditions	↓	4	4	3	5
14		1%	1		Noise	↓	5	5	4	5
15		1%	1		Vibration	↓	5	5	4	5
16		5%	4	**Design**	Scalability/flexibility	↑	5	1	2	5
17		4%	3		Dimensions	↓	3	2	3	5
18		5%	4		Reliability	↑	5	5	4	4
19		5%	4		Need of after treatment	↓	5	5	2	5
20		6%	5	**Costs**	Lifetime	↑	5	4	3	5
21		4%	3		Capex	↓	3	4	3	3
22		6%	5		Opex	↓	3	3	3	4
23		4%	3		Catalyst	↓	4	4	2	4
24		6%	5	**Technology**	Availability	↑	5	5	5	1
25		5%	4		Know-how	↑	5	5	5	2
					Target (1-5)		3,0	3,0	3,0	3,0
					Rating		4,36	4,18	3,21	4,05
					Relative Weight		27,6%	26,4%	20,3%	25,6%
					Weight Chart					
					Position		1	2	4	3

Appendix C - Process Flow Diagram

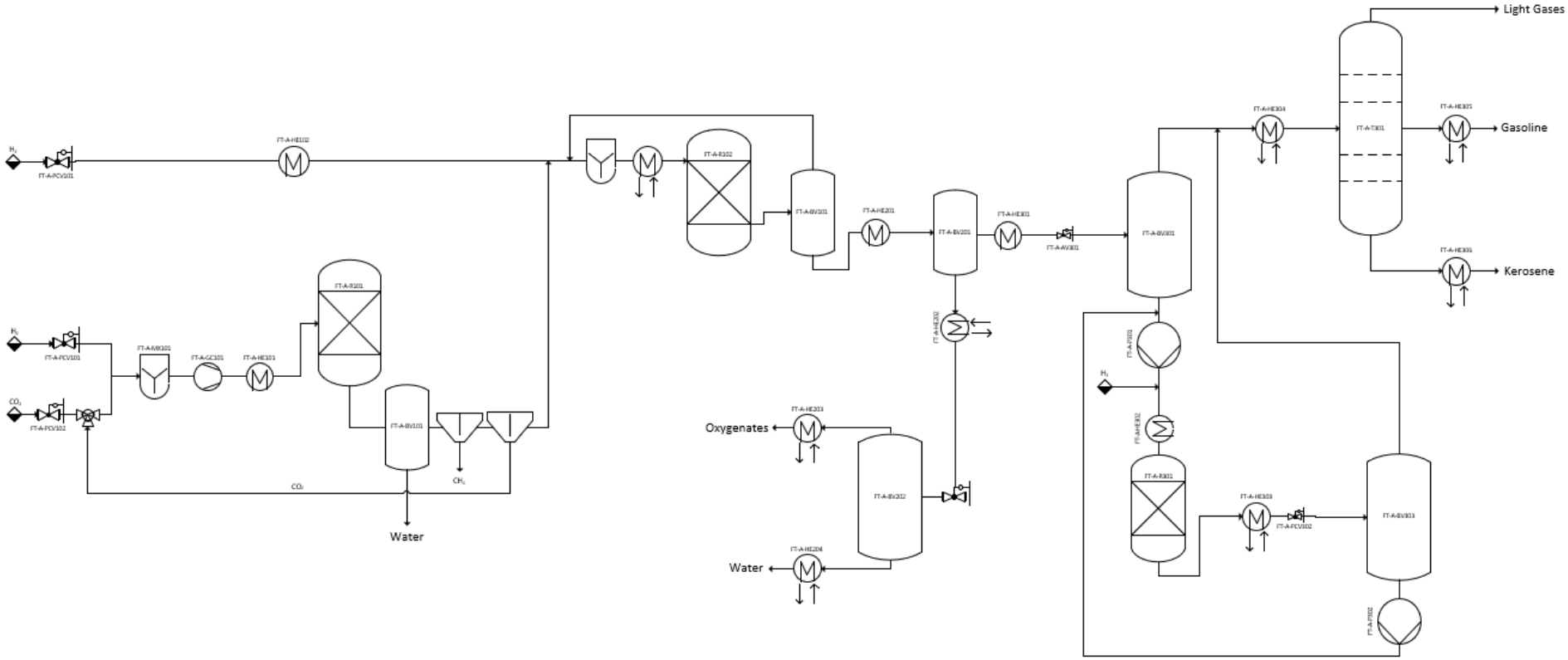

Appendix D - Kinetic Mechanisms Deduction

As explained in the Chapter 3.1.1, the rate equations were derived considering the mechanisms and the assumptions defined by the authors of the model.

Therefore, there are presented the steps to derive the rate equations for the rWGS reaction, CO_2 and CO methanation, since in the literature, the presented equations are the WGS reaction, SRM to CO_2 and SRM to CO, respectively, the reverse reactions.

A.1 CO Methanation Reaction

The relevant elementary steps are explicit below:

$$H_2 + * \rightleftarrows H_2 * \qquad K_{H_2}$$

$$H_2 * + * \rightleftarrows 2H * \qquad {}^{1}/_{K_H}$$

$$CO + * \rightleftarrows CO * \qquad K_{CO}$$

$$\mathbf{CO} * + \mathbf{H} * \underset{\mathbf{k_{-A}}}{\overset{\mathbf{k_A}}{\rightleftarrows}} \mathbf{CHO} * + * \qquad K_A$$

$$CHO * + H * \rightleftarrows CH_2O * + * \qquad K_B$$

$$CH_2O * + * \rightleftarrows CH_2 * + O * \qquad K_C$$

$$CH_2 * + H * \rightleftarrows CH_3 * + * \qquad K_D$$

$$CH_3 * + H * \rightleftarrows CH_4 * + * \qquad K_E$$

$$CH_4 * \rightleftarrows CH_4 + * \qquad {}^{1}/_{K_{CH_4}}$$

$$O * + H_2 \rightleftarrows H_2O + * \qquad {}^{1}/_{K_{H_2O}}$$

Where k_A and k_{-A} are the velocity constants of the direct reaction and reverse reaction of the rate-determining step, respectively.

The velocity of the rate-determining step is given as:

$$r_3 = k_A[CO *][H *] - k_{-A}[CHO *][*] = k_E\left([CO *]H[*] - \frac{[CHO *][*]}{K_A}\right)$$

All the other steps, as referred, are considered to be in quasi-equilibrium, whereby the concentration of the species can be determined through the equilibrium constants, as shown below:

$$K_{H_2} = \frac{[H_2 *]}{P_{H_2}[*]} \quad \leftrightarrow \quad [H_2 *] = K_{H_2} P_{H_2} [*]$$

$$\frac{1}{K_H} = \frac{[H *]^2}{[H_2 *][*]} \quad \leftrightarrow \quad [H *] = \left(\frac{[H_2 *][*]}{K_H}\right)^{1/2} = \left(\frac{K_{H_2}}{K_H} P_{H_2}\right)^{1/2} [*]$$

$$K_{CO} = \frac{[CO *]}{P_{CO}[*]} \quad \leftrightarrow \quad [CO *] = K_{CO} P_{CO} [*]$$

$$K_B = \frac{[CH_2O *][*]}{[CHO *][H *]} \quad \leftrightarrow \quad [CHO *] = \frac{{K_H}^{1.5} K_{CH_4} K_{H_2O}}{K_B K_C K_D K_E {K_{H_2}}^{1.5}} \frac{P_{CH_4} P_{H_2O}}{{P_{H_2}}^{2.5}} [*]$$

$$K_C = \frac{[CH_2 *][O *]}{[CH_2O *][*]} \quad \leftrightarrow \quad [CH_2O *] = \frac{K_H K_{CH_4} K_{H_2O}}{K_C K_D K_E K_{H_2}} \frac{P_{CH_4}}{{P_{H_2}}^{2.5}} [*]$$

$$K_D = \frac{[CH_3 *][*]}{[CH_2 *][H *]} \quad \leftrightarrow \quad [CH_2 *] = \frac{K_H K_{CH_4}}{K_D K_E K_{H_2}} \frac{P_{CH_4} P_{H_2O}}{{P_{H_2}}^{2}} [*]$$

$$K_E = \frac{[CH_4 *][*]}{[CH_3 *][H *]} \quad \leftrightarrow \quad [CH_3 *] = \frac{{K_H}^{0.5} K_{CH_4}}{K_E {K_{H_2}}^{0.5}} \frac{P_{CH_4}}{{P_{H_2}}^{0.5}} [*]$$

$$\frac{1}{K_{CH_4}} = \frac{P_{CH_4}[*]}{[CH_4 *]} \quad \leftrightarrow \quad [CH_4 *] = K_{CH_4} P_{CH_4} [*]$$

$$\frac{1}{K_{H_2O}} = \frac{P_{H_2O}[*]}{[O *] P_{H_2}} \quad \leftrightarrow \quad [O *] = K_{H_2O} \frac{P_{H_2O}}{P_{H_2}} [*]$$

To determine $[*]$, it is required the mass of the active center in the catalyst, where Δ represents the total concentration of active centers.

$$\Delta = [*] + [O *] + [CH_4 *] + [CH_3 *] + [CH_2 *] + [CH_2O *] + [CHO *] + [CO *] + [H *] + [H_2 *]$$

As the concentrations of the carbon-containing ($CH_3 *$, $CH_2 *$, $CH *$and $C *$) radicals are much lower than the total concentration of the active sites, it is disregard in the calculations, and so:

$$\Delta = [*] + [O *] + [CH_4 *] + [CO *] + [H *] + [H_2 *]$$

As the H atoms are immediately released to the gaseous phase, the term $[\mathrm{H}*]\sim 0$, and the concentration of the active sites is described as:

$$[*] = \frac{\Delta}{1 + \frac{[\mathrm{O}*]}{[*]} + \frac{[\mathrm{CH_4}*]}{[*]} + \frac{[\mathrm{CO}*]}{[*]} + \frac{[\mathrm{H_2}*]}{[*]}}$$

$$[*] = \frac{\Delta}{1 + \mathrm{K_{CO}P_{CO}} + \mathrm{K_{H_2}P_{H_2}} + \mathrm{K_{CH_4}P_{CH_4}} + \mathrm{K_{H_2O}}\frac{\mathrm{P_{H_2O}}}{\mathrm{P_{H_2}}}}$$

Replacing the previous expression on the velocity expression:

$$\mathrm{r_3} = \mathrm{k_A}[*]^2\left(\frac{[\mathrm{CO}*][\mathrm{H}*]}{[*]^2} - \frac{[\mathrm{CHO}*][*]}{[*]^2\mathrm{K_A}}\right)$$

$$\mathrm{r_3} = \frac{\mathrm{k_A}\Delta^2\left(\mathrm{K_{CO}P_{CO}}[*]\frac{\mathrm{K_{H_2}}^{0.5}}{\mathrm{K_H}^{0.5}}\mathrm{P_{H_2}}^{0.5}[*]\frac{1}{[*]^2} - \frac{\mathrm{K_H}^{1.5}\mathrm{K_{CH_4}K_{H_2O}}}{\mathrm{K_B K_C K_D K_E K_{H_2}}^{1.5}}\frac{\mathrm{P_{CH_4}P_{H_2O}}}{\mathrm{P_{H_2}}^{2.5}}[*][*]\frac{1}{[*]^2}\frac{1}{\mathrm{K_A}}\right)}{\left(1 + \mathrm{K_{CO}P_{CO}} + \mathrm{K_{H_2}P_{H_2}} + \mathrm{K_{CH_4}P_{CH_4}} + \mathrm{K_{H_2O}}\frac{\mathrm{P_{H_2O}}}{\mathrm{P_{H_2}}}\right)^2}$$

$$\mathrm{r_3} = \frac{\mathrm{k_A}\Delta^2\frac{\mathrm{K_B K_C K_D K_E K_{H_2}}^{1.5}}{\mathrm{K_H}^{1.5}\mathrm{K_{CH_4}K_{H_2O}}}\left(\frac{\mathrm{K_B K_C K_D K_E K_{H_2}}^{1.5}\mathrm{K_{CO}K_{H_2}}^{0.5}}{\mathrm{K_H}^{1.5}\mathrm{K_{CH_4}K_{H_2O}K_H}^{0.5}}\mathrm{P_{H_2}}^{0.5}\mathrm{P_{CO}} - \frac{\mathrm{P_{CH_4}P_{H_2O}}}{\mathrm{P_{H_2}}^{2.5}}\frac{1}{\mathrm{K_A}}\right)}{\left(1 + \mathrm{K_{CO}P_{CO}} + \mathrm{K_{H_2}P_{H_2}} + \mathrm{K_{CH_4}P_{CH_4}} + \mathrm{K_{H_2O}}\frac{\mathrm{P_{H_2O}}}{\mathrm{P_{H_2}}}\right)^2}$$

$$\mathrm{r_3} = \frac{\mathrm{k_3}\left(\frac{\mathrm{P_{CO}}\mathrm{P_{H_2}}^{0.5}}{\mathrm{K_3}} - \frac{\mathrm{P_{CH_4}P_{H_2O}}}{\mathrm{P_{H_2}}^{2.5}}\right)}{\left(1 + \mathrm{K_{CO}P_{CO}} + \mathrm{K_{H_2}P_{H_2}} + \mathrm{K_{CH_4}P_{CH_4}} + \mathrm{K_{H_2O}}\frac{\mathrm{P_{H_2O}}}{\mathrm{P_{H_2}}}\right)^2}$$

$$\mathrm{r_3} = \frac{\frac{\mathrm{k_3}}{\mathrm{P_{H_2}}^{2.5}}\left(\frac{\mathrm{P_{CO}}\mathrm{P_{H_2}}^{3}}{\mathrm{K_3}} - \mathrm{P_{CH_4}P_{H_2O}}\right)}{\left(1 + \mathrm{K_{CO}P_{CO}} + \mathrm{K_{H_2}P_{H_2}} + \mathrm{K_{CH_4}P_{CH_4}} + \mathrm{K_{H_2O}}\frac{\mathrm{P_{H_2O}}}{\mathrm{P_{H_2}}}\right)^2}$$

A.2 CO_2 Methanation Reaction

The relevant elementary steps are explicit below:

$$\mathrm{H_2} + * \rightleftarrows \mathrm{H_2}* \qquad \mathrm{K_{H_2}}$$

$$\mathrm{H_2}* + * \rightleftarrows 2\mathrm{H}* \qquad {}^{1}/_{\mathrm{K_H}}$$

$$CO_2 + * \rightleftarrows CO_2 * \qquad K_{CO_2}$$

$$\mathbf{CO_2 * + H *} \underset{\mathbf{k_{-A}}}{\overset{\mathbf{k_A}}{\rightleftarrows}} \mathbf{CHO * + O *} \qquad K_A$$

$$COH * + H * \rightleftarrows CH_2O * + * \qquad K_B$$

$$CH_2O * + * \rightleftarrows CH_2 * + O * \qquad K_C$$

$$CH_2 * + H * \rightleftarrows CH_3 * + * \qquad K_D$$

$$CH_3 * + H * \rightleftarrows CH_4 * + * \qquad K_E$$

$$CH_4 * \rightleftarrows CH_4 + * \qquad {}^{1}/_{K_{CH_4}}$$

$$O * + H_2 \rightleftarrows H_2O + * \qquad {}^{1}/_{K_{H_2O}}$$

As in the previous case for the CO methanation, k_A and k_{-A} are the velocity constants of the direct reaction and reverse reaction of the rate-determining step, respectively.

For this reaction, the velocity of the rate-determining step is given as:

$$r_2 = k_A[CO_2 *][H *] - k_{-A}[CHO *][O *] = k_A\left([CO_2 *][H *] - \frac{[CHO *][O *]}{K_A}\right)$$

The intermediate steps, as in the previous demonstration, are in quasi-equilibrium and the concentration of the species can be determined through the equilibrium constants, as shown below:

$$K_{H_2} = \frac{[H_2 *]}{P_{H_2}[*]} \quad \leftrightarrow \quad [H_2 *] = K_{H_2}P_{H_2}[*]$$

$$\frac{1}{K_H} = \frac{[H *]^2}{[H_2 *][*]} \quad \leftrightarrow \quad [H *] = \left(\frac{K_{H_2}}{K_H}P_{H_2}\right)^{1/2}[*]$$

$$K_{CO_2} = \frac{[CO_2 *]}{P_{CO_2}[*]} \quad \leftrightarrow \quad [CO_2 *] = K_{CO_2}P_{CO_2}[*]$$

$$K_B = \frac{[CH_2O *][*]}{[CHO *][H *]} \quad \leftrightarrow \quad [CHO *] = \frac{K_{CH_4}{K_H}^{1.5}K_{H_2O}}{K_BK_CK_DK_E{K_{H_2}}^{1.5}}\frac{P_{CH_4}P_{H_2O}}{{P_{H_2}}^{2.5}}[*]$$

$$K_C = \frac{[CH_2 *][O *]}{[CH_2O *][*]} \quad \leftrightarrow \quad [CH_2O *] = \frac{K_{CH_4}K_HK_{H_2O}}{K_CK_DK_EK_{H_2}}\frac{P_{CH_4}P_{H_2O}}{{P_{H_2}}^{2}}[*]$$

$$K_D = \frac{[CH_3 *][*]}{[CH_2 *][H *]} \quad \leftrightarrow \quad [CH_2 *] = \frac{K_{CH_4}K_H}{K_DK_EK_{H_2}}\frac{P_{CH_4}}{P_{H_2}}[*]$$

$$K_E = \frac{[CH_4\,*][*]}{[CH_3\,*][H\,*]} \qquad \leftrightarrow \qquad [CH_3\,*] = \frac{K_{CH_4}{K_H}^{0.5}}{K_E{K_{H_2}}^{0.5}}\frac{P_{CH_4}}{{P_{H_2}}^{0.5}}[*]$$

$$\frac{1}{K_{CH_4}} = \frac{P_{CH_4}[*]}{[CH_4\,*]} \qquad \leftrightarrow \qquad [CH_4\,*] = K_{CH_4}P_{CH_4}[*]$$

$$\frac{1}{K_{H_2O}} = \frac{P_{H_2O}[*]}{[O\,*]P_{H_2}} \qquad \leftrightarrow \qquad [O\,*] = K_{H_2O}\frac{P_{H_2O}}{P_{H_2}}[*]$$

As the reactive system occurs at the same and in the same active centers of the nickel catalyst, the total concentration of the active centers is equal for the three reactions, and so, the expression remains the same.

Replacing the previous expression on the velocity expression:

$$r_2 = k_A\left([CO_2\,*][H\,*] - \frac{[CHO\,*][O\,*]}{K_A}\right)$$

$$r_2 = \frac{k_A\Delta^2\left(\frac{K_{CO_2}{K_{H_2}}^{0.5}}{{K_H}^{0.5}}{P_{CO_2}{P_{H_2}}^{0.5}}[*][*]\frac{1}{[*]^2} - \frac{K_{CH_4}{K_H}^{1.5}{K_{H_2O}}^2}{K_BK_CK_DK_E{K_{H_2}}^{1.5}}\frac{P_{CH_4}{P_{H_2O}}^2}{{P_{H_2}}^{3.5}}[*][*]\frac{1}{[*]^2}\frac{1}{K_A}\right)}{\left(1 + K_{CO}P_{CO} + K_{H_2}P_{H_2} + K_{CH_4}P_{CH_4} + K_{H_2O}\frac{P_{H_2O}}{P_{H_2}}\right)^2}$$

$$r_2 = \frac{k_A\Delta^2\frac{K_BK_CK_DK_E{K_{H_2}}^{1.5}}{K_{CH_4}{K_H}^{1.5}{K_{H_2O}}^2}\left(\frac{K_BK_CK_DK_E{K_{H_2}}^{1.5}K_{CO_2}{K_{H_2}}^{0.5}}{K_{CH_4}{K_H}^{1.5}{K_{H_2O}}^2{K_H}^{0.5}}{P_{CO_2}{P_{H_2}}^{0.5}} - \frac{P_{CH_4}{P_{H_2O}}^2}{{P_{H_2}}^{3.5}}\frac{1}{K_A}\right)}{\left(1 + K_{CO}P_{CO} + K_{H_2}P_{H_2} + K_{CH_4}P_{CH_4} + K_{H_2O}\frac{P_{H_2O}}{P_{H_2}}\right)^2}$$

$$r_2 = \frac{k_2\left(\frac{P_{CO}{P_{H_2}}^{0.5}}{K_2} - \frac{P_{CH_4}{P_{H_2O}}^2}{{P_{H_2}}^{3.5}}\right)}{\left(1 + K_{CO}P_{CO} + K_{H_2}P_{H_2} + K_{CH_4}P_{CH_4} + K_{H_2O}\frac{P_{H_2O}}{P_{H_2}}\right)^2}$$

$$r_2 = \frac{\frac{k_2}{{P_{H_2}}^{3.5}}\left(\frac{P_{CO}{P_{H_2}}^{4}}{K_2} - P_{CH_4}{P_{H_2O}}^2\right)}{\left(1 + K_{CO}P_{CO} + K_{H_2}P_{H_2} + K_{CH_4}P_{CH_4} + K_{H_2O}\frac{P_{H_2O}}{P_{H_2}}\right)^2}$$

A.3 rWGS Reaction

The relevant elementary steps for the rWGS reaction are:

$$CO_2 + * \rightleftarrows CO_2 * \qquad K_{CO_2}$$

$$\mathbf{CO_2} * + * \underset{\mathbf{k_{-A}}}{\overset{\mathbf{k_A}}{\rightleftarrows}} \mathbf{CO} * + \mathbf{O} * \qquad K_A$$

$$CO * \rightleftarrows CO + * \qquad {}^{1}/_{K_{CO}}$$

$$O * + H_2 \rightleftarrows H_2O + * \qquad {}^{1}/_{K_{H_2O}}$$

As in the previous case for the CO methanation, k_A and k_{-A} are the velocity constants of the direct reaction and reverse reaction of the rate-determining step, respectively.

For this reaction, the velocity of the rate-determining step is given as:

$$r_1 = k_A[CO_2 *][*] - k_{-A}[CO *][O *] = k_A\left([CO_2 *][H *] - \frac{[CO *][O *]}{K_A}\right)$$

The intermediate steps, as in the previous demonstration, are in quasi-equilibrium and the concentration of the species can be determined through the equilibrium constants, as shown below:

$$K_{CO_2} = \frac{[CO_2 *]}{P_{CO_2}[*]} \qquad \leftrightarrow \qquad [CO_2 *] = K_{CO_2}P_{CO_2}[*]$$

$$\frac{1}{K_{CO}} = \frac{P_{CO}[*]}{[CO *]} \qquad \leftrightarrow \qquad [CO *] = K_{CO}P_{CO}[*]$$

$$\frac{1}{K_{H_2O}} = \frac{P_{H_2O}[*]}{[O *]P_{H_2}} \qquad \leftrightarrow \qquad [O *] = K_{H_2O}\frac{P_{H_2O}}{P_{H_2}}[*]$$

As the reactive system occurs at the same and in the same active centers of the nickel catalyst, the total concentration of the active centers is equal for the three reactions, and so, the expression remains the same.

Replacing the previous expression on the velocity expression:

$$r_1 = k_A\left([CO_2 *][*] - \frac{[CO *][O *]}{K_A}\right)$$

$$r_1 = \frac{k_A\Delta^2\left(K_{CO_2}P_{CO_2}[*][*]\frac{1}{[*]^2} - K_{CO}K_{H_2O}\frac{P_{CO}P_{H_2O}}{P_{H_2}}[*][*]\frac{1}{[*]^2}\frac{1}{K_A}\right)}{\left(1 + K_{CO}P_{CO} + K_{H_2}P_{H_2} + K_{CH_4}P_{CH_4} + K_{H_2O}\frac{P_{H_2O}}{P_{H_2}}\right)^2}$$

$$r_1 = \frac{k_A \frac{\Delta^2}{K_{CO} K_{H_2O}} \left(K_{CO_2} K_{CO} K_{H_2O} P_{CO_2} - \frac{P_{CO} P_{H_2O}}{P_{H_2}} \frac{1}{K_A} \right)}{\left(1 + K_{CO} P_{CO} + K_{H_2} P_{H_2} + K_{CH_4} P_{CH_4} + K_{H_2O} \frac{P_{H_2O}}{P_{H_2}} \right)^2}$$

$$r_1 = \frac{k_1 \left(\frac{P_{CO}}{K_1} - \frac{P_{CO} P_{H_2O}}{P_{H_2}} \right)}{\left(1 + K_{CO} P_{CO} + K_{H_2} P_{H_2} + K_{CH_4} P_{CH_4} + K_{H_2O} \frac{P_{H_2O}}{P_{H_2}} \right)^2}$$

$$r_1 = \frac{\frac{k_1}{P_{H_2}} \left(\frac{P_{CO} P_{H_2}}{K_1} - P_{CO} P_{H_2O} \right)}{\left(1 + K_{CO} P_{CO} + K_{H_2} P_{H_2} + K_{CH_4} P_{CH_4} + K_{H_2O} \frac{P_{H_2O}}{P_{H_2}} \right)^2}$$

Appendix E - Equilibrium Conversion

The considered reactions are described according to the extension as shown next.

$$CO_2 + H_2 \rightleftarrows CO + H_2O \qquad \xi_1$$

$$CO_2 + 4H_2 \rightleftarrows CH_4 + 2H_2O \qquad \xi_2$$

$$CO + 3H_2 \rightleftarrows CH_4 + H_2O \qquad \xi_3$$

$$CO_2 + 2H_2 \rightleftarrows C + 2H_2O \qquad \xi_4$$

$$2CO \rightleftarrows C + CO_2 \qquad \xi_5$$

From the reactions above, it is possible to define the molar balance of each compound according to the extension of the reactions, according to the next Eq. X.

$$f_i = f_{i,0} + \sum \upsilon_i \xi_j$$

$$f_{CO_2} = f_{CO_2,0} - \xi_1 - \xi_2 - \xi_4 + \xi_5$$

$$f_{H_2} = f_{H_2,0} - \xi_1 - 4\xi_2 - 3\xi_3 - 2\xi_4$$

$$f_{CO} = 0 + \xi_1 - \xi_3 - 2\xi_5$$

$$f_{H_2O} = 0 + \xi_1 + 2\xi_2 + \xi_3 + 2\xi_4$$

$$f_{CH_4} = 0 + \xi_2 + \xi_3$$

$$f_C = 0 + \xi_4 + \xi_5$$

The sum of the previous molar balances defines the total mole balance:

$$f_T = f_{CO_2,0} + f_{H_2,0} - \xi_2 - 2\xi_3$$

At this point, it is possible to define the fraction of each compound, x_i, dividing the respective molar balance equation for the total balance equation.

$$x_{CO_2} = \frac{f_{CO_2,0} - \xi_1 - \xi_2 - \xi_4 + \xi_5}{f_{CO_2,0} + f_{H_2,0} - \xi_2 - 2\xi_3}$$

$$x_{H_2} = \frac{f_{H_2,0} - \xi_1 - 4\xi_2 - 3\xi_3 - 2\xi_4}{f_{CO_2,0} + f_{H_2,0} - \xi_2 - 2\xi_3}$$

$$x_{CO} = \frac{\xi_1 - \xi_3 - 2\xi_5}{f_{CO_2,0} + f_{H_2,0} - \xi_2 - 2\xi_3}$$

$$x_{H_2O} = \frac{\xi_1 + 2\xi_2 + \xi_3 + 2\xi_4}{f_{CO_2,0} + f_{H_2,0} - \xi_2 - 2\xi_3}$$

$$x_{CH_4} = \frac{\xi_2 + \xi_3}{f_{CO_2,0} + f_{H_2,0} - \xi_2 - 2\xi_3}$$

$$x_C = \frac{\xi_4 + \xi_5}{f_{CO_2,0} + f_{H_2,0} - \xi_2 - 2\xi_3}$$

It is known that the equilibrium constant can be determined by:

$$K_{eq} = P^{\sum \upsilon_i} \prod x_i^{\upsilon_i}$$

Where υ_i is the stoichiometric coefficient and so $\sum \upsilon_i$ gives the stoichiometric balance for each reaction.

For each reaction, it is determined that:

$$K_{eq_1} = P^0 \frac{x_{CO} x_{H_2O}}{x_{CO_2} x_{H_2}} = \frac{x_{CO} x_{H_2O}}{x_{CO_2} x_{H_2}}$$

$$K_{eq_2} = P^{-2} \frac{x_{CH_4} {x_{H_2O}}^2}{x_{CO_2} {x_{H_2}}^4} = \frac{1}{P^2} \frac{x_{CH_4} {x_{H_2O}}^2}{x_{CO_2} {x_{H_2}}^4}$$

$$K_{eq_3} = P^{-2} \frac{x_{CH_4} x_{H_2O}}{x_{CO} {x_{H_2}}^3} = \frac{1}{P^2} \frac{x_{CH_4} x_{H_2O}}{x_{CO} {x_{H_2}}^3}$$

$$K_{eq_4} = P^0 \frac{x_C {x_{H_2O}}^2}{x_{CO_2} {x_{H_2}}^2} = \frac{x_C {x_{H_2O}}^2}{x_{CO_2} {x_{H_2}}^2}$$

$$K_{eq_5} = P^0 \frac{{x_{CO}}^2}{x_{CO_2} x_C} = \frac{{x_{CO}}^2}{x_{CO_2} x_C}$$

In order to be possible to obtain the extents of the reaction, it is necessary to determine the equilibrium constant for each reaction. Using the correlation presented in the Eq. 3.9 and according to the parameters founded in the literature, it is possible to determine the equilibrium constant for each reaction. The data used and the obtained results are presented in the next Table 15.

Table 15. Equilibrium constant parameters and final value for 973 K.

	λ_1	λ_2	λ_3	K_{eq}
1. rWGS	-191 928.1	-3 937.4	3.8143	0.110554
2. CO_2 Methanation	-730 726	24 125.3	-26.9616	491.537
3. CO Methanation	-538 798.1	28 062.7	-30.7759	3692.59
4. Bosch	-121 003.4	16 573.0	-17.3858	421.141
5. Boudouard	70 924.7	20 510.4	-21.2000	3809.74

Defined the equilibrium constant value for each reaction, at the defined temperature of 973 K, it is now possible to use the solver tool do determine the extent of the reactions, defining the restriction that the equilibrium constants dependent of the extent values have to be equal to the determined equilibrium constants by the Eq. 3.9.